Chapter 7

Experiments with partial barriers.

This chapter explores a slightly different aspect of barrier blocked flows, by investigating flows where the system is only partially blocked, by a barrier of height h, where the ratio of the barrier height to the depth of the annulus, $h/d < 1$. These partial barriers otherwise occupy the entire radial width of the annulus cavity. By varying h/d, the related problem of how the changes in the flow, which occur between the fully blocked and unblocked cases, can be investigated.

Kester (1966) performed a series of investigations using thin barriers with a whole range of heights. He concluded that there was a relatively abrupt transition which occured when $h \approx 0.7d$. For $h/d < 0.7$ Kester felt that the flow was essentially unblocked, while for $h/d > 0.7$ the flows seemed to be more like blocked flows. However Kester's measurements suffered from significant errors; notably his failure to calibrate his instruments before use. Consequently it is no surprise to find that his heat transport measurements found no difference between the heat transport in fully blocked and unblocked systems. His visual results however may be more reliable. He found that with barriers of negligible azimuthal width, the surface flow pattern (traced using aluminium powder) remained the same as that in an unblocked annulus (including the appearance of regular waves) for barriers

less than $0.7d$ high. Higher barriers caused noticeable effects to the waves, and the appearance of a topographically forced wave. It was the effect on the surface wave pattern that caused him to conclude that the transition was abrupt, and occured when $h \approx 0.7d$.

Leach (1975) explored the effect of partial barriers on flow in a differentially heated rotating annulus. He was not interested in the transition between blocked and unblocked flows, but he did make several observations with a barrier of height $d/3$ and azimuthal width $\Delta\phi = \pi/15$, which rested on the bottom of the annulus. This barrier was very similar to the 1/3 barrier described in §2.1.1 and *Figure 2.2(b)*, which had an azimuthal width of $\Delta\phi = \pi/6$ (i.e. 30°). Leach observed a closed circulation downstream of his topography, and he also concluded that the barriers tended to supress the free baroclinic waves he found in the system. Under certain circumstances these waves would break up as they crossed the partial barrier, and reform about 90° downstream. He mentions that strong prograde flow was to be expected in such systems because of the drag exerted by the flow on the topography, by considering the torque balance on the annulus in the steady–state. Finally he attributed the increase in measured heat transport above that observed in the unobstructed annulus to be due to the topographically forced wave seen over the barrier. Leach was unable to observe any increase in Nu associated with the height of his partial barriers because of the errors in his measurements.

In this chapter the results of transport measurements made using a large barrier (with $h = \frac{2}{3}d$) and a small barrier (with $h = \frac{1}{3}d$) are reported. Also velocity measurements with two barriers which both had the same height, $h = \frac{2}{3}d$ but differing azimuthal widths (30° and 60°) have been made. The velocity and temperature results were then compared with results from fully blocked and un-

blocked systems to look for any similarities between those systems. The heat transport measurements were sufficiently accurate to distinguish between the different heat transport characteristics found with the barriers of $h = \frac{2}{3}d$ and $h = \frac{1}{3}d$. Though only two heights of barriers were used, it has been possible to use the heat transport results to draw certain conclusions about the nature of the transition from blocked to unblocked flows, as a function of h/d. The barriers used for the measurements reported in this chapter are described in §2.1.1 (experimental configurations numbers 5 to 7), and examples of the barriers are shown in *Figure 2.2 (a), (b).*

The experimental results are given in §7.1; §7.1.1 and §7.1.2 deal with the $h/d = 2/3$, 30° wide barrier, and §7.1.3 the $h/d = 2/3$, 60° wide barrier. The temperature measurements made with the $h/d = 1/3$ barrier are given in §7.1.4, with a summary of all the results in §7.1.5.

The results are discussed in §7.2. A simplified flow pattern is given (§7.2.1) and the η-circulation seen in the blocked region of the two-thirds barrier flow is considered in §7.2.2. Estimates are made of the heat advection in the unblocked regions above the barriers in §7.2.3. In §7.2.4 measurements of v are used to estimate the radial temperature gradient in the unblocked region for the $h/d = 2/3$, 30° wide barrier. The conclusions are given in §7.3, while §7.4 suggests further measurements that could be made to extend the work.

7.1 Experimental results.

7.1.1 Velocity measurements with a $\frac{2}{3}d$, 30° wide barrier.

A regime diagram showing the values of τ and Θ for all the velocity measurements taken with the $h/d = 2/3$, 30° wide partial barrier is shown in *Figure 7.1.* It can be seen that waves occur for $\Theta \lesssim 1.0$ and for $\tau \gtrsim 3.0 \times 10^6$. Thus the region of

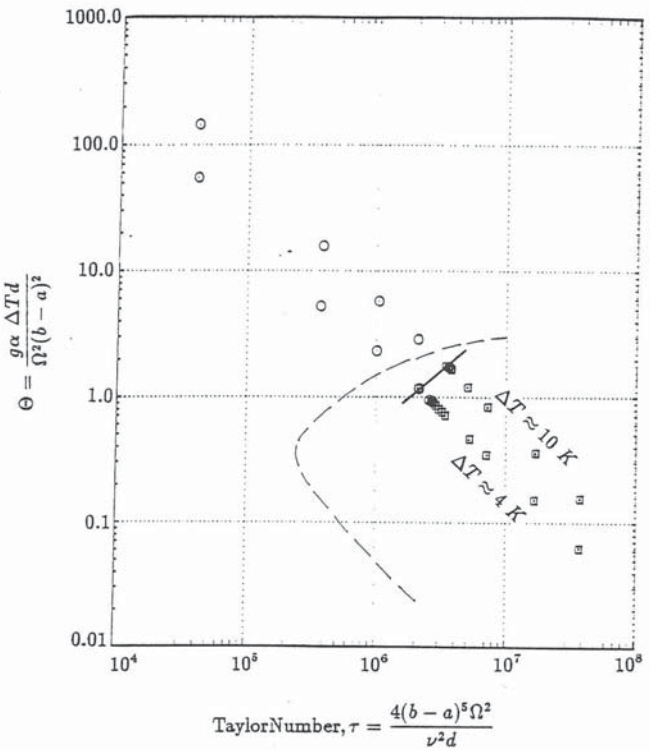

FIGURE 7.1: Regime diagram showing the values of τ and Θ for velocity runs 284-312, the measurements with a two-thirds partial barrier. The circles show results where there were no waves in the system, and the squares when waves were present. The dashed line indicates the approximate location of the transition for the onset of baroclinic waves for an unblocked annulus, such as that used by *Fowlis and Hide (1965).* The location of the dashed line was obtained from D.W.Johnson (private communication), while the solid line indicates the location of the transition for the onset of waves in the present experiments.

(r, Θ) space where wave-like activity was seen was smaller than for an unblocked annulus, but greater than for a fully blocked annulus. The waves were time-dependent and aperiodic, appearing to drift around the annulus in the prograde sense. Location of the transition was quite difficult because near the transition there were transient waves which often took several hours to die away. In this case the flows were recorded on a time–lapse video recorder and later replayed upto 72 times faster, since the waves near the transition were often rather weak. While the use of the video recorder assisted in the location of the transition it was still very difficult to pinpoint it with much accuracy.

Figures 7.2-7.4 show measurements of horizontal velocities interpolated onto a regular grid of vectors in a (r, ϕ)-plane. *Figure 7.2* shows the velocities at $\Omega = 0.48\ rad.sec^{-1}$ and $\Delta T = 4.00\ K$. Above the barrier, in (a) and (b), there is evidence of a topographically forced wave. At the top of the barrier (c), there are signs of radially inwards flow (by the sides of the barrier) and in (e) there are some signs of radially outwards flow. In (d), about half-way up the barrier, there is some prograde flow by the outer wall, and possibly retrograde flow by the inner wall. The strong prograde flow in (c) is probably related to the flow in (a) and (b).

Figure 7.3 shows the fluid motions at $\Omega = 1.08\ rad.sec^{-1}$ and $\Delta T = 3.86\ K$. The topographically forced wave in (a) and (b) is more pronounced, though the prograde motion above the barrier is weaker. There are some signs of radially inwards motion in (c) and outwards motion in (e). In (c) and (d), prograde motion can be seen by the outer wall and retrograde motion by the inner wall. In (d) this motion is stronger than that seen in *Figure 7.2*.

Figure 7.4 shows results for $\Omega = 2.93\ rad.sec^{-1}$ and $\Delta T = 3.98\ K$. The prograde motion in (a) and (b) is weaker still, except possibly by the inner and

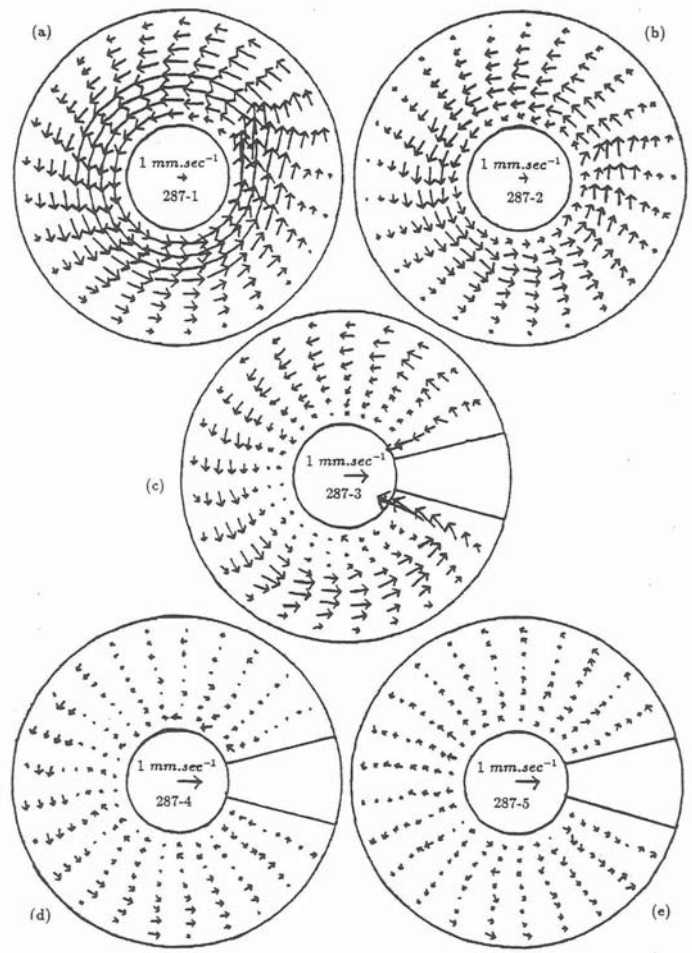

FIGURE 7.2: Horizontal velocity field data taken by VVAS, reprojected onto a regular grid, for the annulus with a two-thirds partial barrier. The location of the barrier is indicated by the blocked out region in (c)-(e). The flows at various heights above the base of the annulus are shown; (a) 124 *mm*, (b) 97 *mm*, (c) 70 *mm*, (d) 43 *mm* and (e) 16 *mm*. Data from run 287, $\Omega = 0.48\ rad.sec^{-1}$, $\Delta T = 4.00\ K$. The central arrow in each case depicts 1 $mm.sec^{-1}$. The figure shows the mean flow over six minutes. Strong prograde flow can be seen in (a) and (b), with a slight topographically forced wave as fluid passed over the barrier. In (c) and (d) prograde flow can be seen by the outer wall. There is some evidence of radially outward flow in (e). The depth of the annulus was $d = 140\ mm$.

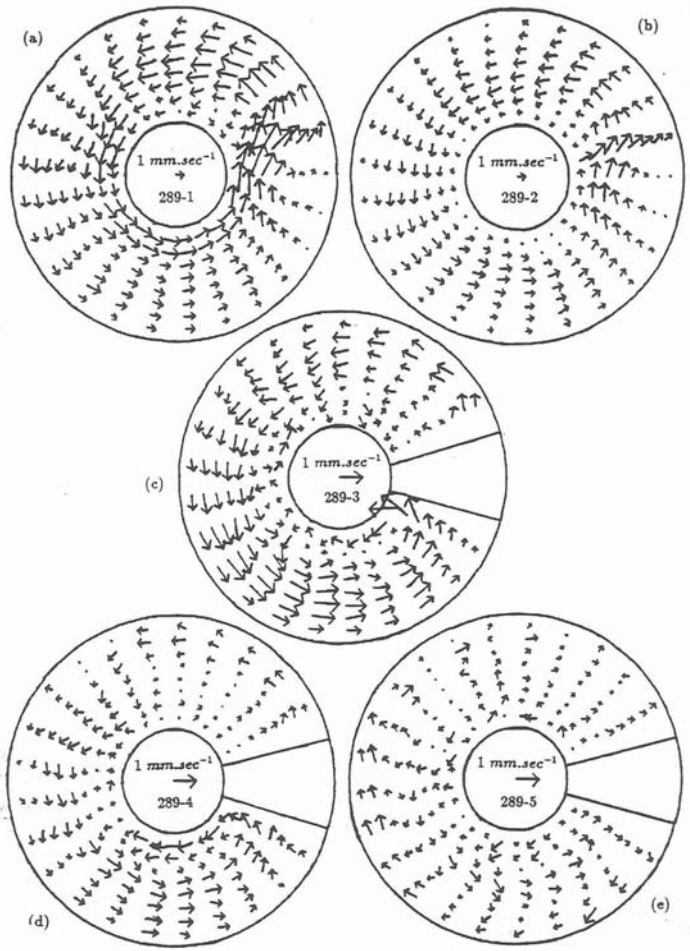

FIGURE 7.3: Horizontal velocity field data taken by VVAS, reprojected onto a regular grid, for the annulus with a two-thirds partial barrier. The location of the barrier is indicated by the blocked out region in (c)-(e). The flows at various heights above the base of the annulus are shown; (a) 124 *mm*, (b) 97 *mm*, (c) 70 *mm*, (d) 43 *mm* and (e) 16 *mm*. Data from run 289, $\Omega = 1.08$ *rad.sec*$^{-1}$, $\Delta T = 3.86$ *K*. The central arrow in each case depicts 1 *mm.sec*$^{-1}$. The figure shows the mean flow over six minutes. Strong prograde flow can be seen in (a) and (b), with a topographically forced wave as fluid passed over the barrier. In (c) and (d) prograde flow can be seen by the outer wall, with some retrograde flow by the inner wall. There is some evidence of radially outward flow in (e). The depth of the annulus was $d = 140$ *mm*.

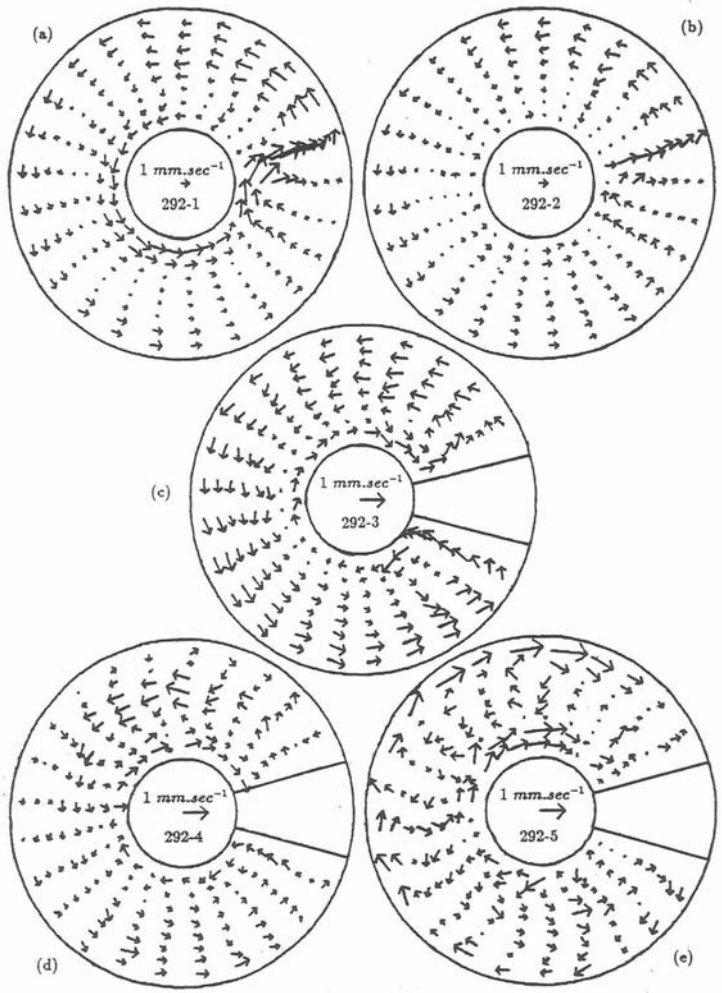

FIGURE 7.4: Horizontal velocity field data taken by VVAS, reprojected onto a regular grid, for the annulus with a two-thirds partial barrier. The location of the barrier is indicated by the blocked out region in (c)-(e). The flows at various heights above the base of the annulus are shown; (a) 124 *mm*, (b) 97 *mm*, (c) 70 *mm*, (d) 43 *mm* and (e) 16 *mm*. Data from run 292, $\Omega = 2.93$ *rad.sec*$^{-1}$, $\Delta T = 3.98$ *K*. The central arrow in each case depicts 1 *mm.sec*$^{-1}$. The figure shows the mean flow over six minutes. Prograde flow can be seen in (a) and (b), with a topographically forced wave as fluid passed over the barrier. In (c) and (d) prograde flow can be seen by the outer wall, with some retrograde flow by the inner wall. There is some evidence of radially outward flow in (e). The depth of the annulus was $d = 140$ *mm*.

outer walls. The topographically forced wave is clearly visible. Flow in (c) and (d) seems to be dominated by prograde motion towards the outer wall and retrograde motion by the inner wall. There is still some radially outwards flow in (e). *Figures 7.3 (a), (b)* and *7.4 (a), (b)* show signs of the closed circulation downstream of the barrier mentioned by *Leach (1975)* (see also the start of this chapter).

Mean (over azimuth) u contours are shown in *Figure 7.5* in an (r, z) plane. (a)-(c) in *Figure 7.5* correspond to the data shown in *Figures 7.2-7.4*. Since the barrier was 93 *mm* high, its top was just below the 97 *mm* mark on each of the vertical axes. In (a) there is very clearly a radial overturning over the range of height blocked by the barrier. This can still be seen in (b), and to a lesser extent in (c). Comparison with *Figure 3.5* shows there to be considerable similarities between the blocked part of the partial barrier system and the fully blocked system. In (a) the contours are very evenly spaced with z in the lower half of the annulus at mid-radius, suggesting a region where $\partial u/\partial z \approx constant$. The fact that there were regions where the flow was similar to the fully blocked results is likely to be significant in terms of heat advection by the fluid.

The azimuthal mean of v is shown in *Figure 7.6*, where contours of v are plotted in an (r, z)-plane. The strong prograde flow above the barrier can be seen, which drops off with increasing Ω. There is some evidence for an increasingly strong shear of v with r as Ω increases, but it is difficult to separate this from the prograde flow above the barrier.

Figure 7.7 shows contours of v in a (ϕ, z)-plane at mid-radius. (a) and (b) illustrate how the system appears to split into two regions, roughly corresponding with above and below the top of the barrier. Above the barrier, flow appears to be dominated by azimuthal motion, and below it, radial motion. However at

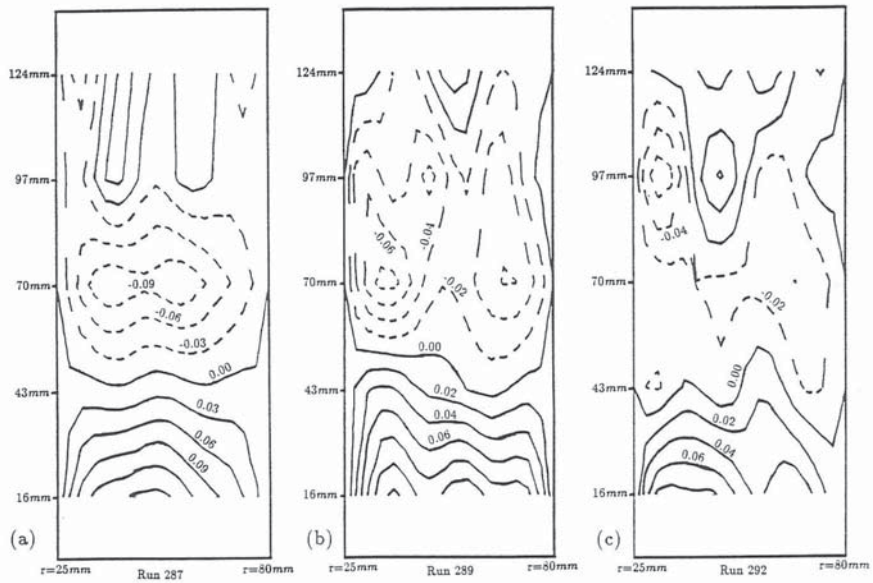

FIGURE 7.5: The figures show contours of u in $mm.sec^{-1}$ in an (r, z) plane for the annulus with a two-thirds partial barrier. Solid contours represent radially outwards flow and dashed contours, inwards flow. (a) Run 287, $\Delta T = 4.00\ K$, $\Omega = 0.481\ rad.sec^{-1}$, (b) run 289, $\Delta T = 3.86\ K$, $\Omega = 1.078\ rad.sec^{-1}$, and (c) run 292, $\Delta T = 3.98\ K$, $\Omega = 2.928\ rad.sec^{-1}$. The barrier rested on the bottom of the annulus and had a height of 93 *mm*. In all cases a clear shear of radial velocity with height can be seen over the range blocked by the barrier.

higher Ω above the barrier v gets weaker and below the top of the barrier u also decreases, so that this split may become less pronounced with increasing Ω.

Table 7.1 summarizes the velocity results with the $h/d = 2/3$, 30° wide barrier.

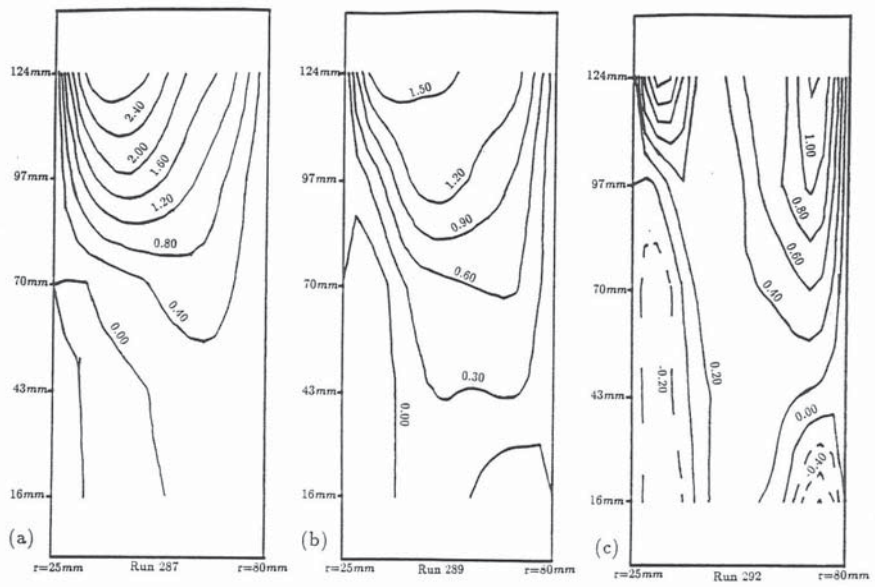

FIGURE 7.6: The figures show contours of mean v in $mm.sec^{-1}$ in an (r, z) plane for the annulus with a two-thirds partial barrier. Solid contours represent prograde flow and dashed contours, retrograde flow. (a) Run 287, $\Delta T = 4.00\ K$, $\Omega = 0.481\ rad.sec^{-1}$, (b) run 289, $\Delta T = 3.86\ K$, $\Omega = 1.078\ rad.sec^{-1}$, and (c) run 292, $\Delta T = 3.98\ K$, $\Omega = 2.928\ rad.sec^{-1}$. The barrier rested on the bottom of the annulus and had a height of 93 mm. Strong prograde flow can be seen above the barrier, while at lower levels there is some evidence of a ζ type circulation.

7.1.2 Temperature measurements with a $\frac{2}{3}d$, 30° wide barrier.

A regime diagram showing the values of τ and Θ for all the temperature and heat transport measurements made with a $h/d = 2/3$, 30° wide partial barrier is shown in *Figure 7.8*. The transition for the onset of time-dependent aperiodic waves is seen to occur at about the same values of τ and Θ as indicated by *Figure 7.1*. The differences in the transitions recorded by the two techniques of visual and temperature measurements are attributed to the difficulties in locating

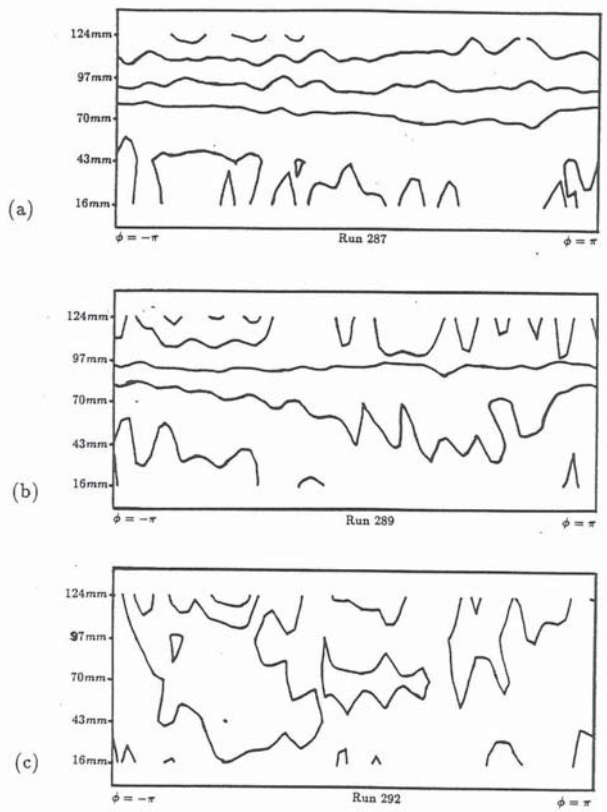

FIGURE 7.7: The figures show contours of v in $mm.sec^{-1}$ in an (ϕ, z) plane for the annulus with a two-thirds partial barrier. Solid contours represent prograde flow and dashed contours, retrograde flow. (a) Run 287, $\Delta T = 4.00\ K$, $\Omega = 0.481\ rad.sec^{-1}$, contour interval 0.70 $mm.sec^{-1}$, (b) run 289, $\Delta T = 3.86\ K$, $\Omega = 1.078\ rad.sec^{-1}$, contour interval 0.60 $mm.sec^{-1}$, and (c) run 292, $\Delta T = 3.98\ K$, $\Omega = 2.928\ rad.sec^{-1}$, contour interval 0.40 $mm.sec^{-1}$. The barrier rested on the bottom of the annulus and had a height of 93 mm. Strong prograde flow can be seen above the barrier in (a) and (b), which decreases significantly with Ω.

Run No	ΔT K	Ω $rad.sec^{-1}$	Prandtl No	Θ	Taylor No	Flow type*
283	4.19	0.875	14.2	7.46×10^{-1}	3.31×10^{6}	waves
284	3.94	0.867	14.2	7.15×10^{-1}	3.25×10^{6}	waves
285	3.77	0.096	14.2	5.53×10^{1}	4.01×10^{4}	no waves
286	3.20	0.289	14.2	5.23	3.60×10^{5}	no waves
287	4.00	0.481	14.2	2.36	1.00×10^{6}	no waves
288	4.00	0.685	14.2	1.16	2.03×10^{6}	no waves
289	3.86	1.078	14.2	4.53×10^{-1}	5.02×10^{6}	waves
290	4.06	1.267	14.2	3.45×10^{-1}	6.93×10^{6}	waves
291	4.23	1.952	14.2	1.51×10^{-1}	1.65×10^{7}	waves
292	3.98	2.928	14.2	6.33×10^{-2}	3.70×10^{7}	waves
293	9.98	0.097	14.2	1.46×10^{2}	4.03×10^{4}	no waves
294	9.96	0.294	14.2	1.58×10^{1}	3.72×10^{5}	no waves
295	9.99	0.489	14.2	5.69	1.03×10^{6}	no waves
296	9.99	0.685	14.2	2.90	2.03×10^{6}	no waves
297	10.01	0.875	14.2	1.78	3.31×10^{6}	waves
298	10.02	1.063	14.2	1.21	4.88×10^{6}	waves
299	10.01	1.275	14.2	8.40×10^{-1}	7.02×10^{6}	waves
300	9.94	1.961	14.2	3.52×10^{-1}	1.66×10^{7}	waves
301	9.95	2.944	14.2	1.57×10^{-1}	3.74×10^{7}	waves
302	3.98	0.844	14.2	7.62×10^{-1}	3.08×10^{6}	waves
303	4.03	0.786	14.2	8.90×10^{-1}	2.67×10^{6}	waves
304	4.06	0.686	14.2	1.17	2.04×10^{6}	no waves
305	4.02	0.736	14.2	1.01	2.40×10^{6}	no waves
306	4.00	0.756	14.2	9.56×10^{-1}	2.47×10^{6}	no waves
307	4.02	0.765	14.2	9.36×10^{-1}	2.53×10^{6}	waves
308	4.02	0.775	14.2	9.12×10^{-1}	2.60×10^{6}	waves
309	4.00	0.785	14.2	8.86×10^{-1}	2.66×10^{6}	waves
310	3.96	0.794	14.2	8.56×10^{-1}	2.73×10^{6}	waves
311	4.11	0.805	14.2	8.63×10^{-1}	2.88×10^{6}	waves
312	3.93	0.824	14.2	7.89×10^{-1}	2.93×10^{6}	waves

* 'no waves' means that only the topographically forced wave was present, while 'waves' indicates that other waves were present apart from the stationary topographically forced wave.

TABLE 7.1: Velocity measurements with a two-thirds, 30° wide barrier.

what appeared to be a rather more gradual transition than in an unblocked annulus. It is also possible that the thermocouple ring influenced the location of the transition, particularly because the waves near the transition were rather weak (see §2.1.4).

Figure 7.9 shows the fluid temperature measured by the thermocouple ring at $\bar{r}$ and $z = 0$. The centre of the barrier was placed at $\phi = \pm\pi$. Plots of temperature are given at three values of Ω for each of the two values of ΔT used.

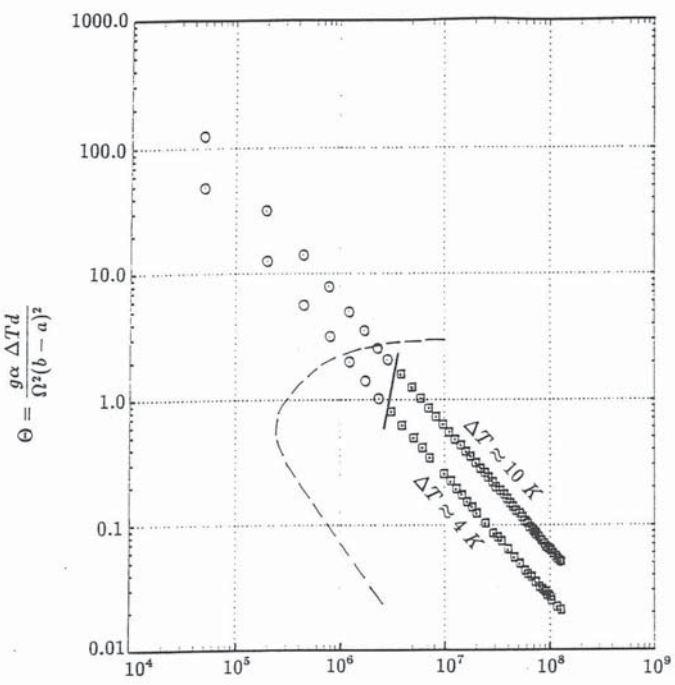

FIGURE 7.8: Regime diagram showing the values of τ and Θ for runs 126-227, the measurements with a two-thirds partial barrier. The circles show results where temperature measurements indicated there were no waves in the system, and the squares when waves were present. The dashed line indicates the approximate location of the transition for the onset of baroclinic waves for an unblocked annulus, such as that used by *Fowlis and Hide (1965)*. The location of the dashed line was obtained from D.W.Johnson (private communication), while the solid line indicates the transition for the onset of waves in the present experiments.

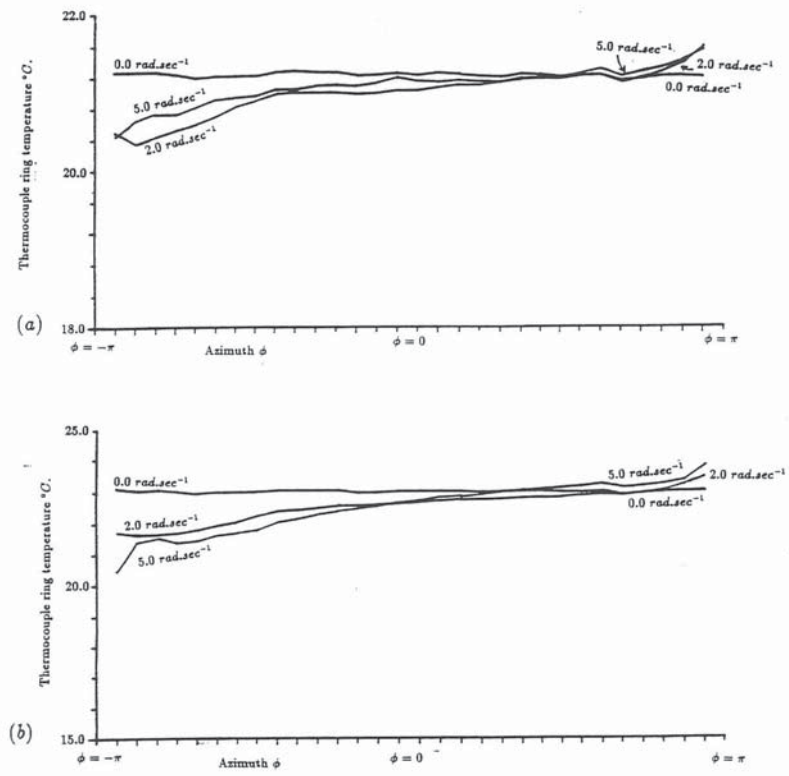

FIGURE 7.9: Measurements showing the temperature of ring thermocouple against ϕ for $\Omega = 0.0, 2.0$ and $5.0\ rad.sec^{-1}$, for the system with a two-thirds partial barrier. Each of the scale markings along the horizontal axis shows the location of one of the thermocouples in the ring. A straight line is drawn between each point to serve as a guide for the eye. The barrier was located with its centre at $\phi = \pm\pi$. The standard errors were (a) $0.0095°C$, and (b) $0.0049°C$. For (a) $\Delta T \approx 4\ K$ and (b) $\Delta T \approx 10\ K$. Note that ΔT_B was defined as the difference between the maximum and minimum thermocouple ring temperatures. As the figures show these were usually at or near the sides of the barrier.

It can be seen that $T(\bar{r}, z = 0; \phi, t)$ is quite linearly dependent on ϕ. It is quite possible that the sharp up or down–turns in the temperatures near to the sides of the barrier are due to the effect of the topographically forced wave, since the top of the barrier was only 2.3cm above the thermocouple ring.

The dependence of ΔT_B on Ω can be seen in *Figure 7.10*, the results are generally quite similar to those with the full insulating barrier (*Figure 3.10*), except that they are significantly larger and at $\Delta T \approx 4\ K$, ΔT_B drops off significantly for $\Omega \gtrsim 3.6\ rad.sec^{-1}$. At $\Delta T \approx 10\ K$, ΔT_B shows more structure than *Figure 3.10 (b)*. ΔT_B reaches a maximum value of about 34 to 40% of ΔT at $\Theta \sim 3.8 \times 10^{-2}$ to 9.7×10^{-2}.

The total heat transport of the fluid, as expressed by the Nusselt number, $\mathrm{Nu}(\Omega)$ is shown in *Figure 7.11*. The plots show $\mathrm{Nu}(\Omega)/\mathrm{Nu}(\Omega = 0)$ against Ω, for the two values of ΔT used. Both sets of results show that the heat transport by the fluid decreased to about 91-96% of its non-rotating value, before increasing slightly at larger values of Ω. The one rather high value measured at $\Omega = 1.0\ rad.sec^{-1}$ in (b) is regarded as suspect due to the large number of measurements that contradict it.

Tables 7.2 and *7.3* summarize the heat transport and temperature measurements with the two-thirds depth, 30° wide partial barrier.

7.1.3 Velocity measurements with a $\frac{2}{3}d$, 60° wide barrier.

The measurements made with a $h/d = 2/3$, 60° wide partial barrier were made by eye or using a time-lapse video cassette recorder. Few measurements were taken, but they were sufficient to determine the location of the transition for the onset of aperiodic time-dependent waves at $\Delta T \approx 4\ K$. The results are shown as a regime diagram in *Figure 7.12*. Near the transition transient waves often took several hours to die away, making precise location of the transition difficult. A

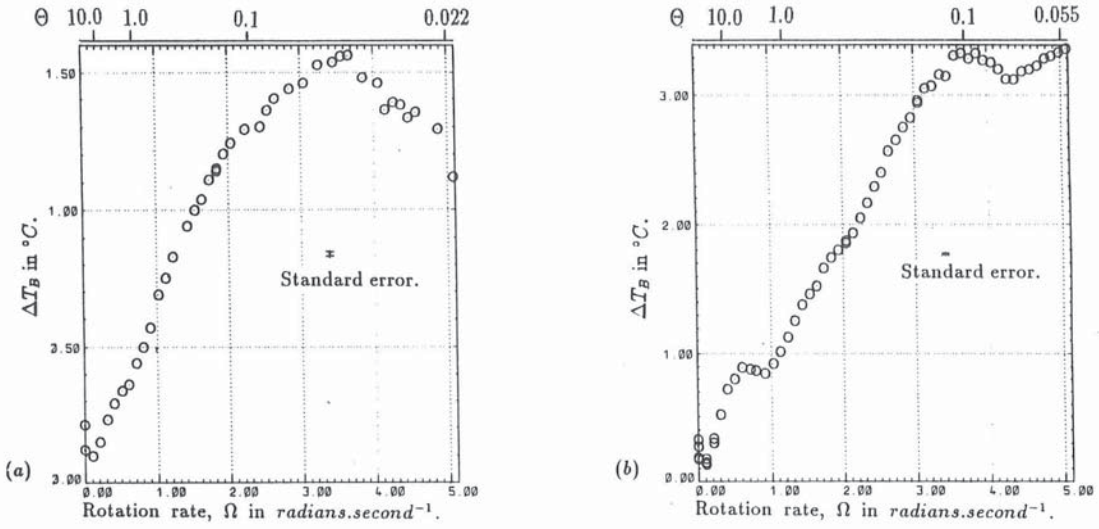

FIGURE 7.10: Measurements showing the dependence of ΔT_B on Ω for the system with a two-thirds partial barrier. (a) $\Delta T \approx 4\ K$, (b) $\Delta T \approx 10\ K$.

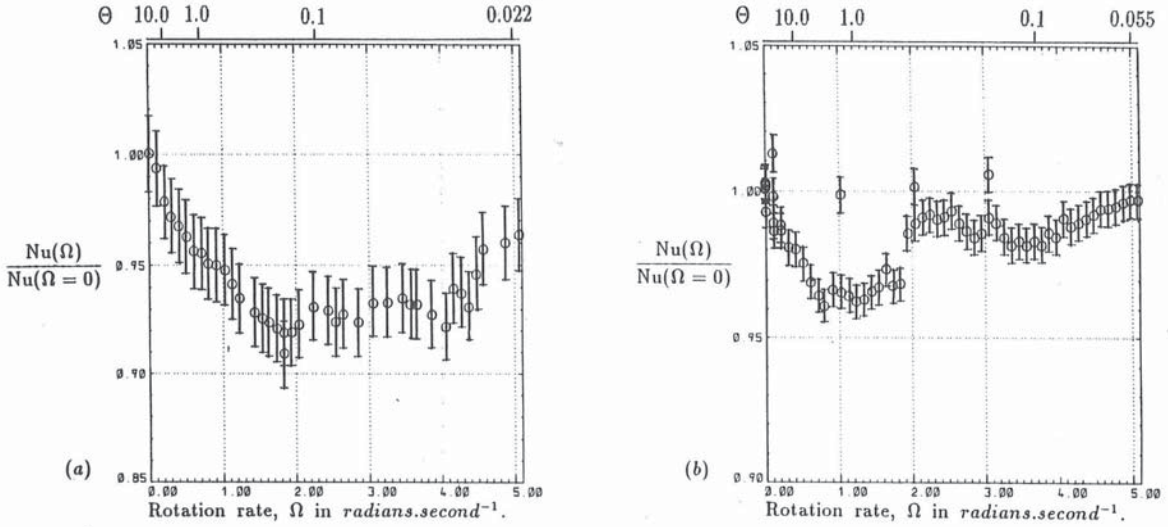

FIGURE 7.11: Measurements showing the dependence of Nusselt number, $Nu(\Omega)$, divided by $Nu(\Omega=0)$, on Ω, for the system with a two-thirds partial barrier. (a) $\Delta T \approx 4\ K$, (b) $\Delta T \approx 10\ K$.

Run No	Ω $rad.sec^{-1}$	ΔT K	ΔT_{BAR} K	Prandtl No	Θ	Taylor No	Rayleigh No	Ekman No	$H_{conductive}$ $watts$	H_{total} $watts$	Nusselt No
126	0.000	3.99	0.12	13.95	∞	0	8.48×10^6	0	1.48	15.92	10.77
127	0.000	4.11	0.21	13.77	∞	0	8.76×10^6	0	1.53	16.44	10.77
128	0.102	4.01	0.10	13.77	4.94×10^1	5.02×10^4	8.53×10^6	2.88×10^{-3}	1.49	15.92	10.70
129	0.203	4.02	0.15	13.77	1.25×10^1	1.99×10^5	8.55×10^6	1.45×10^{-3}	1.49	15.72	10.54
130	0.303	4.01	0.23	13.77	5.56	4.46×10^5	8.54×10^6	9.66×10^{-4}	1.49	15.58	10.47
131	0.404	4.02	0.29	13.77	3.15	7.89×10^5	8.56×10^6	7.27×10^{-4}	1.49	15.55	10.42
132	0.505	4.00	0.34	13.77	2.00	1.24×10^6	8.52×10^6	5.80×10^{-4}	1.49	15.41	10.37
133	0.605	4.01	0.36	13.77	1.40	1.77×10^6	8.53×10^6	4.85×10^{-4}	1.49	15.32	10.30
134	0.706	4.01	0.44	13.77	1.03	2.42×10^6	8.53×10^6	4.15×10^{-4}	1.49	15.30	10.29
135	0.806	4.00	0.50	13.77	7.86×10^{-1}	3.15×10^6	8.52×10^6	3.64×10^{-4}	1.49	15.22	10.24
136	0.908	4.00	0.57	13.77	6.20×10^{-1}	3.99×10^6	8.52×10^6	3.23×10^{-4}	1.49	15.21	10.23
137	1.021	4.01	0.69	13.77	4.91×10^{-1}	5.05×10^6	8.54×10^6	2.87×10^{-4}	1.49	15.19	10.21
138	1.122	4.01	0.75	13.77	4.07×10^{-1}	6.10×10^6	8.54×10^6	2.61×10^{-4}	1.49	15.10	10.14
139	1.223	4.01	0.83	13.77	3.42×10^{-1}	7.25×10^6	8.54×10^6	2.40×10^{-4}	1.49	14.99	10.07
140	1.425	4.01	0.94	13.77	2.52×10^{-1}	9.84×10^6	8.55×10^6	2.06×10^{-4}	1.49	14.90	10.00
141	1.527	4.01	1.00	13.77	2.19×10^{-1}	1.13×10^7	8.53×10^6	1.92×10^{-4}	1.49	14.83	9.97
142	1.628	4.00	1.04	13.77	1.92×10^{-1}	1.28×10^7	8.51×10^6	1.80×10^{-4}	1.48	14.76	9.95
143	1.830	4.01	1.15	13.77	1.53×10^{-1}	1.62×10^7	8.53×10^6	1.60×10^{-4}	1.49	14.57	9.79
144	1.729	4.02	1.11	13.77	1.72×10^{-1}	1.45×10^7	8.56×10^6	1.70×10^{-4}	1.49	14.82	9.92
145	2.032	4.01	1.24	13.77	1.24×10^{-1}	2.00×10^7	8.54×10^6	1.44×10^{-4}	1.49	14.81	9.94
146	2.235	4.01	1.29	13.77	1.03×10^{-1}	2.42×10^7	8.55×10^6	1.31×10^{-4}	1.49	14.94	10.03
147	1.828	4.01	1.14	13.77	1.53×10^{-1}	1.62×10^7	8.55×10^6	1.60×10^{-4}	1.49	14.76	9.90
148	1.931	4.01	1.20	13.77	1.37×10^{-1}	1.81×10^7	8.54×10^6	1.52×10^{-4}	1.49	14.75	9.90
149	2.437	3.98	1.30	13.77	8.56×10^{-2}	2.88×10^7	8.48×10^6	1.20×10^{-4}	1.48	14.80	10.01
150	2.537	4.00	1.36	13.77	7.94×10^{-2}	3.12×10^7	8.52×10^6	1.16×10^{-4}	1.49	14.79	9.95

TABLE 7.2: Temperature and heat transport measurements with a two-thirds, 30° wide barrier.

Run No	Ω $rad.sec^{-1}$	ΔT K	ΔT_{BAR} K	Prandtl No	Θ	Taylor No	Rayleigh No	Ekman No	$H_{conductive}$ $watts$	H_{total} $watts$	Nusselt No
151	2.639	4.01	1.40	13.77	7.34×10^{-2}	3.37×10^7	8.53×10^6	1.11×10^{-4}	1.49	14.85	9.99
152	2.843	4.01	1.44	13.77	6.34×10^{-2}	3.92×10^7	8.54×10^6	1.03×10^{-4}	1.49	14.82	9.95
153	3.039	4.01	1.46	13.77	5.54×10^{-2}	4.48×10^7	8.53×10^6	9.65×10^{-5}	1.49	14.95	10.05
154	3.245	4.01	1.53	13.77	4.86×10^{-2}	5.10×10^7	8.54×10^6	9.04×10^{-5}	1.49	14.97	10.05
155	3.449	4.01	1.54	13.77	4.30×10^{-2}	5.77×10^7	8.53×10^6	8.50×10^{-5}	1.49	14.98	10.07
156	3.550	4.02	1.56	13.77	4.07×10^{-2}	6.11×10^7	8.55×10^6	8.26×10^{-5}	1.49	14.97	10.04
157	3.652	4.01	1.56	13.77	3.84×10^{-2}	6.46×10^7	8.54×10^6	8.03×10^{-5}	1.49	14.96	10.04
158	3.854	4.02	1.48	13.77	3.46×10^{-2}	7.20×10^7	8.56×10^6	7.61×10^{-5}	1.49	14.92	9.99
159	4.057	4.07	1.46	13.77	3.16×10^{-2}	7.98×10^7	8.67×10^6	7.23×10^{-5}	1.51	15.01	9.93
160	4.259	4.07	1.39	13.77	2.86×10^{-2}	8.79×10^7	8.66×10^6	6.88×10^{-5}	1.51	15.25	10.10
161	4.463	4.07	1.33	13.77	2.61×10^{-2}	9.65×10^7	8.67×10^6	6.57×10^{-5}	1.51	15.40	10.19
162	4.564	4.07	1.35	13.77	2.49×10^{-2}	1.01×10^8	8.66×10^6	6.43×10^{-5}	1.51	15.57	10.31
163	5.062	4.08	1.12	13.77	2.03×10^{-2}	1.24×10^8	8.69×10^6	5.79×10^{-5}	1.51	15.72	10.38
164	4.869	4.08	1.29	13.77	2.20×10^{-2}	1.15×10^8	8.68×10^6	6.02×10^{-5}	1.51	15.66	10.34
165	4.154	4.07	1.36	13.77	3.01×10^{-2}	8.36×10^7	8.66×10^6	7.06×10^{-5}	1.51	15.28	10.12
166	4.360	4.08	1.38	13.77	2.74×10^{-2}	9.21×10^7	8.68×10^6	6.73×10^{-5}	1.51	15.19	10.03

TABLE 7.2 (continued).

TABLE 7.3: Temperature and heat transport measurements with a two-thirds, 30° wide barrier.

Run No	ΔT K	Ω $rad.sec^{-1}$	ΔT_{BAR} K	Prandtl No	Θ	Taylor No	Rayleigh No	Ekman No	$H_{conductive}$ $watts$	H_{total} $watts$	Nusselt No
167	10.01	0.000	0.33	13.95	∞	0	2.13×10^7	∞	3.70	54.33	14.67
168	10.03	0.000	0.28	13.95	∞	0	2.13×10^7	∞	3.71	53.96	14.53
169	9.97	0.102	0.17	13.95	1.24×10^2	4.91×10^4	2.12×10^7	2.91×10^{-3}	3.69	54.66	14.81
170	10.01	0.102	0.18	13.95	1.24×10^2	4.91×10^4	2.13×10^7	2.91×10^{-3}	3.71	54.11	14.60
171	9.98	0.202	0.30	13.95	3.13×10^1	1.94×10^5	2.12×10^7	1.47×10^{-3}	3.70	53.45	14.46
172	9.90	0.102	0.14	13.95	1.23×10^2	4.90×10^4	2.10×10^7	2.92×10^{-3}	3.67	52.91	14.43
173	9.94	0.102	0.13	13.95	1.23×10^2	4.91×10^4	2.11×10^7	2.91×10^{-3}	3.68	53.24	14.47
174	10.01	0.202	0.33	13.95	3.14×10^1	1.94×10^5	2.13×10^7	1.47×10^{-3}	3.71	53.47	14.43
175	10.01	0.303	0.52	13.95	1.40×10^1	4.36×10^5	2.13×10^7	9.78×10^{-4}	3.71	53.20	14.35
176	10.01	0.403	0.72	13.95	7.92	7.70×10^5	2.13×10^7	7.36×10^{-4}	3.71	53.15	14.34
177	10.02	0.505	0.80	13.95	5.06	1.21×10^6	2.13×10^7	5.88×10^{-4}	3.71	52.94	14.27
178	10.04	0.605	0.89	13.95	3.52	1.73×10^6	2.13×10^7	4.90×10^{-4}	3.72	52.71	14.18
179	10.02	0.707	0.88	13.95	2.58	2.36×10^6	2.13×10^7	4.20×10^{-4}	3.71	52.35	14.11
180	10.02	0.786	0.87	13.95	2.09	2.92×10^6	2.13×10^7	3.77×10^{-4}	3.71	52.17	14.06
181	10.02	0.907	0.84	13.95	1.57	3.90×10^6	2.13×10^7	3.27×10^{-4}	3.71	52.43	14.14
182	10.02	1.017	0.92	13.95	1.25	4.90×10^6	2.13×10^7	2.92×10^{-4}	3.71	52.40	14.13
183	10.02	1.120	1.01	13.95	1.03	5.94×10^6	2.13×10^7	2.65×10^{-4}	3.71	52.33	14.11
184	10.03	1.224	1.13	13.95	8.60×10^{-1}	7.10×10^6	2.13×10^7	2.42×10^{-4}	3.71	52.24	14.08
185	10.00	1.326	1.26	13.95	7.32×10^{-1}	8.32×10^6	2.13×10^7	2.24×10^{-4}	3.70	52.20	14.09
186	10.00	1.426	1.38	13.95	6.32×10^{-1}	9.63×10^6	2.12×10^7	2.08×10^{-4}	3.70	52.30	14.13
187	10.00	1.528	1.46	13.95	5.51×10^{-1}	1.11×10^7	2.12×10^7	1.94×10^{-4}	3.70	52.39	14.15
188	10.00	1.630	1.52	13.95	4.84×10^{-1}	1.26×10^7	2.12×10^7	1.82×10^{-4}	3.70	52.70	14.24
189	10.05	1.730	1.66	13.95	4.31×10^{-1}	1.42×10^7	2.13×10^7	1.71×10^{-4}	3.72	52.65	14.16
190	10.02	1.832	1.74	13.95	3.84×10^{-1}	1.59×10^7	2.13×10^7	1.62×10^{-4}	3.71	52.59	14.17
191	10.02	1.927	1.80	13.95	3.47×10^{-1}	1.76×10^7	2.13×10^7	1.54×10^{-4}	3.71	53.46	14.42
192	9.99	2.034	1.85	13.95	3.11×10^{-1}	1.96×10^7	2.12×10^7	1.46×10^{-4}	3.70	53.52	14.47
193	9.98	2.136	1.93	13.95	2.81×10^{-1}	2.16×10^7	2.12×10^7	1.39×10^{-4}	3.70	53.58	14.50
194	9.98	2.237	2.05	13.95	2.56×10^{-1}	2.37×10^7	2.12×10^7	1.33×10^{-4}	3.69	53.62	14.51
195	9.98	2.338	2.17	13.95	2.35×10^{-1}	2.59×10^7	2.12×10^7	1.27×10^{-4}	3.69	53.55	14.49
196	9.98	2.438	2.30	13.95	2.16×10^{-1}	2.82×10^7	2.12×10^7	1.22×10^{-4}	3.69	53.58	14.50

TABLE 7.3 (continued).

Run No	ΔT K	Ω $rad.sec^{-1}$	ΔT_{BAR} K	Prandtl No	Θ	Taylor No	Rayleigh No	Ekman No	$H_{conductive}$ $watts$	H_{total} $watts$	Nusselt No
197	10.00	2.539	2.41	13.95	1.99×10^{-1}	3.05×10^7	2.12×10^7	1.17×10^{-4}	3.70	53.78	14.53
198	10.04	2.640	2.57	13.95	1.85×10^{-1}	3.30×10^7	2.13×10^7	1.12×10^{-4}	3.72	53.77	14.47
199	10.05	2.740	2.65	13.95	1.72×10^{-1}	3.56×10^7	2.14×10^7	1.08×10^{-4}	3.72	53.69	14.43
200	10.01	2.841	2.75	13.95	1.60×10^{-1}	3.82×10^7	2.13×10^7	1.04×10^{-4}	3.71	53.37	14.40
201	10.01	2.941	2.82	13.95	1.49×10^{-1}	4.10×10^7	2.13×10^7	1.01×10^{-4}	3.71	53.45	14.42
202	10.00	3.043	2.95	13.95	1.39×10^{-1}	4.38×10^7	2.12×10^7	9.75×10^{-5}	3.70	53.71	14.50
203	10.01	3.144	3.05	13.95	1.30×10^{-1}	4.68×10^7	2.13×10^7	9.43×10^{-5}	3.71	53.63	14.47
204	9.97	3.245	3.07	13.95	1.22×10^{-1}	4.99×10^7	2.12×10^7	9.14×10^{-5}	3.69	53.15	14.40
205	9.99	3.346	3.16	13.95	1.15×10^{-1}	5.30×10^7	2.12×10^7	8.87×10^{-5}	3.70	53.09	14.36
206	10.01	3.446	3.15	13.95	1.08×10^{-1}	5.63×10^7	2.13×10^7	8.60×10^{-5}	3.70	53.26	14.38
207	10.00	3.550	3.32	13.95	1.02×10^{-1}	5.97×10^7	2.12×10^7	8.36×10^{-5}	3.70	53.16	14.36
208	10.00	3.651	3.33	13.95	9.65×10^{-2}	6.31×10^7	2.12×10^7	8.13×10^{-5}	3.70	53.23	14.38
209	10.01	3.753	3.29	13.95	9.14×10^{-2}	6.67×10^7	2.13×10^7	7.90×10^{-5}	3.70	53.19	14.36
210	10.01	3.853	3.33	13.95	8.67×10^{-2}	7.03×10^7	2.13×10^7	7.70×10^{-5}	3.70	53.41	14.42
211	10.01	3.955	3.28	13.95	8.23×10^{-2}	7.41×10^7	2.13×10^7	7.50×10^{-5}	3.71	53.36	14.40
212	10.01	4.055	3.26	13.95	7.83×10^{-2}	7.79×10^7	2.13×10^7	7.31×10^{-5}	3.71	53.70	14.49
213	10.02	4.156	3.21	13.95	7.46×10^{-2}	8.18×10^7	2.13×10^7	7.14×10^{-5}	3.71	53.61	14.45
214	10.00	4.258	3.12	13.95	7.09×10^{-2}	8.59×10^7	2.12×10^7	6.97×10^{-5}	3.70	53.55	14.47
215	10.00	4.359	3.12	13.95	6.77×10^{-2}	9.00×10^7	2.12×10^7	6.80×10^{-5}	3.70	53.66	14.49
216	9.99	4.463	3.19	13.95	6.45×10^{-2}	9.43×10^7	2.12×10^7	6.65×10^{-5}	3.70	53.67	14.51
217	10.00	4.564	3.20	13.95	6.17×10^{-2}	9.86×10^7	2.12×10^7	6.50×10^{-5}	3.70	53.85	14.54
218	10.00	4.666	3.23	13.95	5.91×10^{-2}	1.03×10^8	2.12×10^7	6.36×10^{-5}	3.70	53.82	14.54
219	10.00	4.767	3.29	13.95	5.66×10^{-2}	1.08×10^8	2.12×10^7	6.22×10^{-5}	3.70	53.86	14.55
220	10.00	4.868	3.31	13.95	5.42×10^{-2}	1.12×10^8	2.12×10^7	6.09×10^{-5}	3.70	53.91	14.57
221	9.99	4.970	3.34	13.95	5.20×10^{-2}	1.17×10^8	2.12×10^7	5.97×10^{-5}	3.70	53.94	14.58
222	9.99	5.071	3.37	13.95	5.00×10^{-2}	1.22×10^8	2.12×10^7	5.85×10^{-5}	3.70	53.91	14.58
223	10.01	0.000	0.19	13.95	∞	0	2.13×10^7	∞	3.71	54.31	14.65
224	10.01	0.000	0.18	13.95	∞	0	2.13×10^7	∞	3.71	54.32	14.66
225	9.99	1.022	0.92	13.95	1.23	4.95×10^6	2.12×10^7	2.90×10^{-4}	3.70	54.03	14.61
226	10.01	2.035	1.87	13.95	3.11×10^{-1}	1.96×10^7	2.13×10^7	1.46×10^{-4}	3.71	54.32	14.65
227	10.02	3.045	2.93	13.95	1.39×10^{-1}	4.39×10^7	2.13×10^7	9.74×10^{-5}	3.71	54.56	14.71

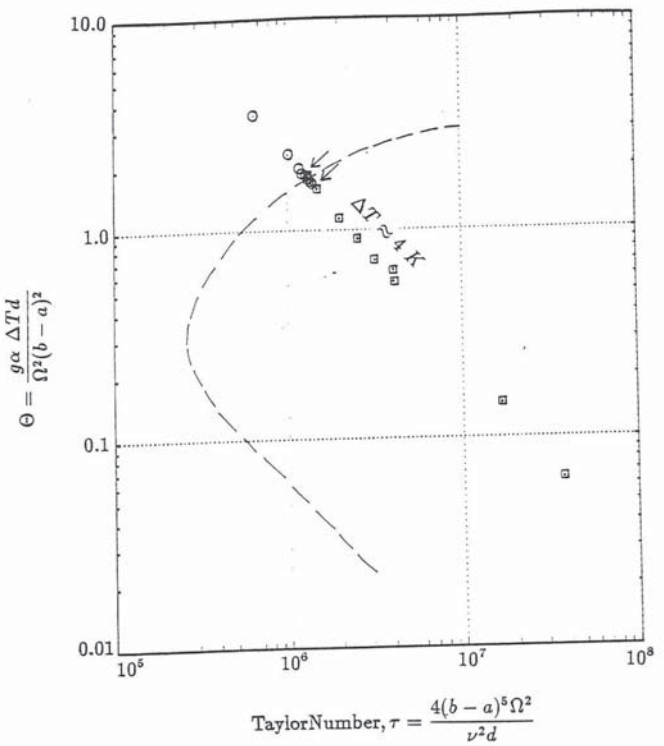

FIGURE 7.12: Regime diagram showing the values of τ and Θ for velocity runs E7-E11 and C399-C414, the measurements with a two-thirds, 60° wide partial barrier. The circles show results where there were no waves in the system, and the squares when waves were present. Near the transition transient waves sometimes took as long as four to five hours to die away, this made location of the transition for the onset of waves rather difficult. The range of measurements between which the transition took place is indicated on the figure by the two arrows. The dashed line indicates the approximate location of the transition for the onset of baroclinic waves for an unblocked annulus, such as that used by *Fowlis and Hide (1965)*. The location of the dashed line was obtained from D.W.Johnson (private communication).

Run No	ΔT K	Ω $rad.sec^{-1}$	Prandtl No	Θ	Taylor No	Flow type*
E7	3.98	0.981	14.4	5.68×10^{-1}	4.07×10^{6}	waves
E8	4.49	0.983	14.4	6.38×10^{-1}	4.08×10^{6}	waves
E9	4.09	1.964	14.4	1.46×10^{-1}	1.63×10^{7}	waves
E10	4.02	2.949	14.4	6.35×10^{-2}	3.67×10^{7}	waves
E11	3.99	0.489	14.4	2.29	1.01×10^{6}	no waves
C399	4.00	0.880	14.4	7.19×10^{-1}	3.23×10^{6}	waves
C400	3.83	0.686	14.4	1.14	1.99×10^{6}	waves
C401	3.97	0.777	14.4	9.04×10^{-1}	2.55×10^{6}	waves
C402	4.01	0.588	14.2	1.58	1.49×10^{6}	waves
C403	3.99	0.392	14.4	3.57	6.48×10^{5}	no waves
C404	4.01	0.489	14.4	2.31	1.01×10^{6}	no waves
C405	3.99	0.538	14.6	1.91	1.20×10^{6}	waves
C406	4.01	0.556	14.6	1.79	1.28×10^{6}	no waves
C407	4.00	0.572	14.6	1.68	1.36×10^{6}	waves
C408	4.02	0.533	14.6	1.95	1.18×10^{6}	no waves
C409	3.92	0.543	14.6	1.84	1.22×10^{6}	no waves
C410	3.97	0.552	14.6	1.80	1.26×10^{6}	no waves
C411	4.01	0.560	14.6	1.78	1.29×10^{6}	no waves
C412	4.13	0.557	14.6	1.85	1.28×10^{6}	waves
C413	4.03	0.574	14.6	1.70	1.36×10^{6}	no waves
C414	4.04	0.582	14.6	1.66	1.39×10^{6}	no waves

* 'no waves' means that only the topographically forced wave was present, while 'waves' indicates that other waves were present apart from the stationary topographically forced wave.

TABLE 7.4: Velocity measurements with a two-thirds, 60° wide barrier.

similar problem was also found with the 30° wide barrier, see §7.1.1 above. The transition for the onset of the waves was found to be the same as for the onset of regular baroclinic waves in an unblocked annulus. This might suggest that the waves seen in the partial barrier systems are baroclinic in nature, and that the effect of the partial barrier is primarily to make the waves aperiodic and time-dependent, and to a lesser extent to affect the location of the transition. However these must be regarded as rather tentative conclusions, without further investigations.

The results with the two-thirds, 60° wide partial barrier are summarized in *Table 7.4*.

7.1.4 Temperature measurements with a $\frac{1}{3}d$, 30° wide barrier.

A regime diagram showing the values of τ and Θ for the temperature and heat transport measurements with a $h/d = 1/3$, 30° wide partial barrier is shown in *Figure 7.13*. The transition for the onset of time-dependent aperiodic waves is seen to occur at $\Theta \sim 1.0$ and $\tau \sim 4.0 \times 10^6$, very similar values to those observed with a two-thirds partial barrier in §7.1.1.

Figure 7.14 shows fluid temperature measured by the thermocouple ring, $T(\bar{r}, z = 0; \phi, t)$. The barrier was placed with its centre at $\phi = \pm\pi$. Because the barrier was only 47 *mm* high, and was placed on the bottom of the annulus, the thermocouple ring passed 23 *mm* above the top of the barrier (since $z = 0$ was defined to be mid-height in the cavity, which was 140 *mm* deep). Thus ΔT_B (defined as the greatest temperature minus the least temperature measured by the thermocouple ring), was probably not a very good estimate of the temperature difference across the barrier. A further problem was that temperature fluctuations in the fluid (caused by the time-dependent aperiodic waves) made the standard error in the average temperatures measured by the thermocouple ring rather large. This was because only the running mean and standard deviations of the thermocouple ring temperatures were recorded, thus the temperatures were time–averaged. In principle the temperature of each thermocouple could be recorded against time for an extended period so that the structure of the aperiodic time–dependent waves could be investigated, however this was not done. The large standard error in the (time–averaged) values of ΔT_B limits their use for quantitative work.

The dependence of ΔT_B on Ω is shown in *Figure 7.15*, which shows plots of ΔT_B against Ω for the two values of ΔT used in the experiments. In general

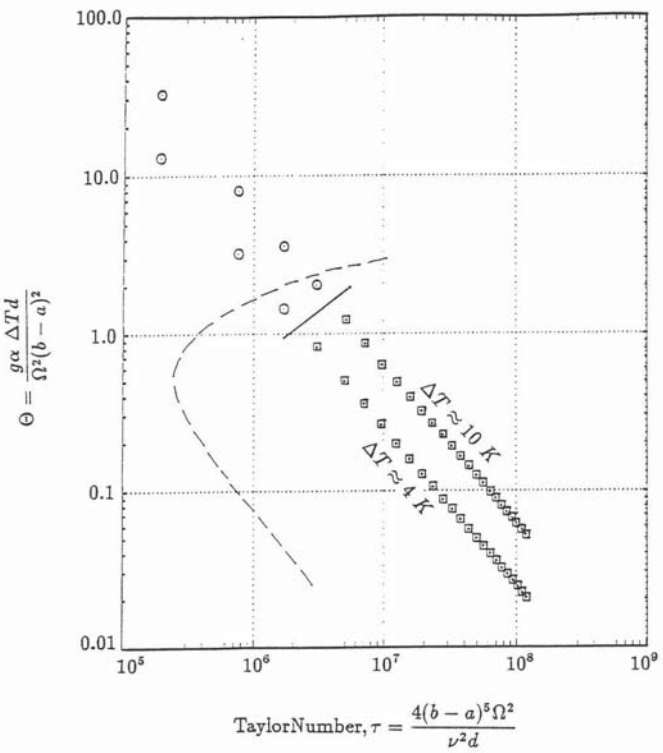

FIGURE 7.13: Regime diagram showing the values of τ and Θ for runs 228-281, the measurements with a one-third partial barrier. The circles show results where temperature measurements indicated there were no waves in the system, and the squares when waves were present. The dashed line indicates the approximate location of the transition for the onset of baroclinic waves for an unblocked annulus, such as that used by *Fowlis and Hide (1965)*. The location of the dashed line was obtained from D.W.Johnson (private communication), while the solid line indicates the transition for the onset of waves in the present experiments.

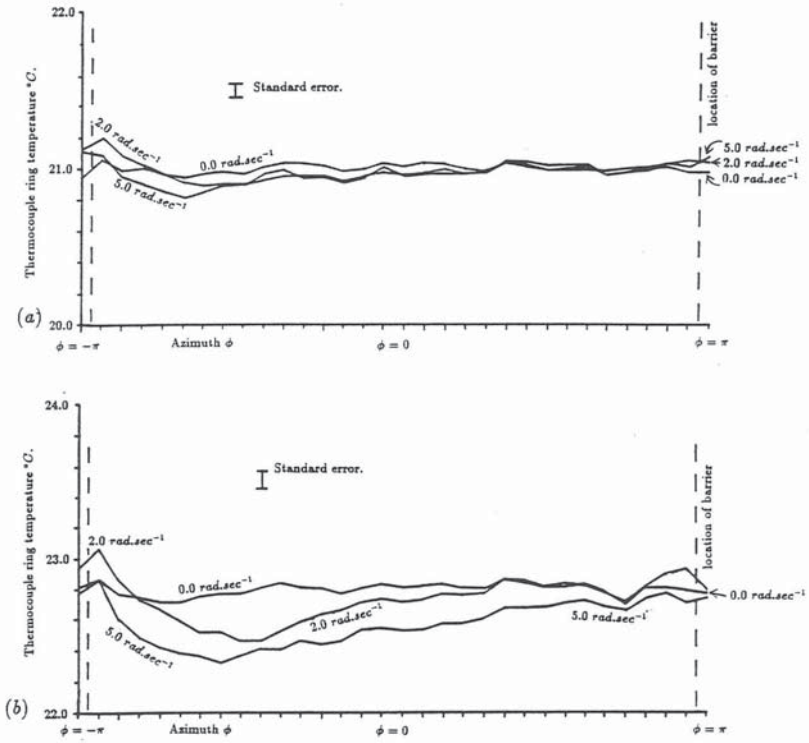

FIGURE 7.14: Measurements showing the temperature of ring thermocouple against ϕ for $\Omega = 0.0, 2.0$ and $5.0\ rad.sec^{-1}$, for the system with a one-third partial barrier. Each of the scale markings along the horizontal axis shows the location of one of the thermocouples in the ring. A straight line is drawn between each point to serve as a guide for the eye. The barrier was located with its centre at $\phi = \pm\pi$. The standard errors were (a) $0.04°C$, and (b) $0.06°C$. For (a) $\Delta T \approx 4\ K$ and (b) $\Delta T \approx 10\ K$. Note that ΔT_B was defined as the difference between the maximum and minimum thermocouple ring temperatures.

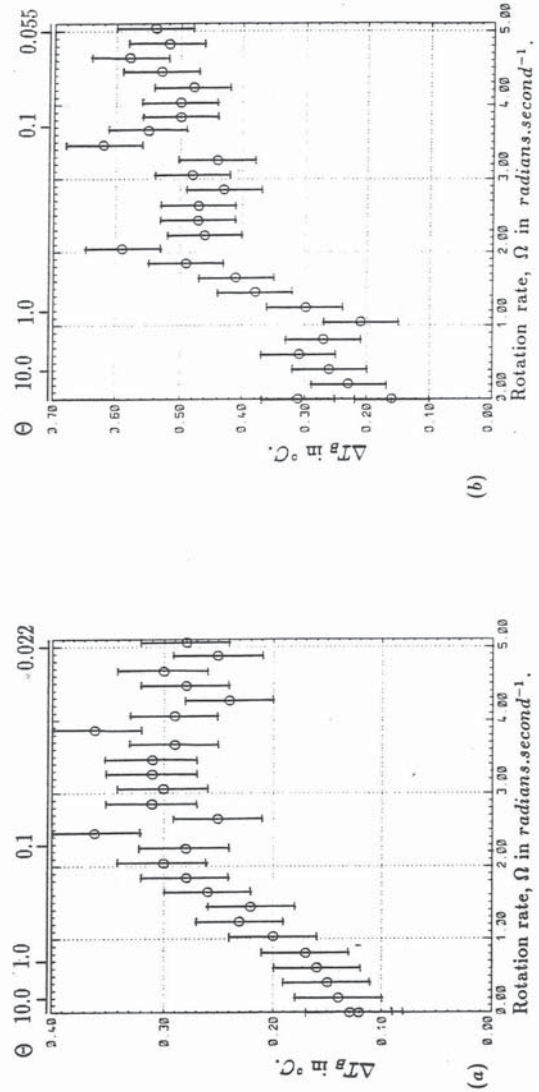

FIGURE 7.15: Measurements showing the dependence of ΔT_B on Ω for the system with a one-third partial barrier. (a) $\Delta T \approx 4\ K$, (b) $\Delta T \approx 10\ K$.

ΔT_B increases with Ω, before levelling off at a value of 5-8% of ΔT at $\Omega \sim 2.0\ rad.sec^{-1}$. These values are very small, and may not be representative of the fluid temperature differences across the barrier, because they were measured at $z = 0$ which was 2.3cm above the top of the barrier.

The total heat transport of the fluid, expressed by the Nusselt number is given in *Figure 7.16.* The heat transport can be seen to drop away rapidly with increasing Ω. The rate of decrease of heat transport with omega slows at $\Omega = 0.8\ rad.sec^{-1}$ in (a), and stops at $\Omega = 1.0\ rad.sec^{-1}$ in (b). These values of Ω correspond closely to the transitions for the onset of waves in each case. In general terms this sort of behaviour is somewhat like that observed in an unblocked annulus. *Hide (1977)* showed results for an unblocked system, where the heat transport fell sharply with increasing Ω until regular waves set in at $\Omega \sim 1.0\ rad.sec^{-1}$. When there were regular waves in the unblocked system the heat transport was about 80% of its non-rotating value. *Figure 7.16* shows that in the $h/d = 1/3$ partial barrier system the lowest heat transport is about 82% at $\Delta T \approx 4\ K$, and 89% at $\Delta T \approx 10\ K$.

The temperature and heat transport results with the $h/d = 1/3$, 30° wide barrier are summarized in *Table 7.5.*

7.1.5 Summary of results.

The transition for the onset of aperiodic time-dependent waves in partial barrier systems was observed to fall between the transitions for the onset of waves (or eddies) in the unblocked and fully blocked annulus systems. The transitions for the $h/d = 1/3$ and $h/d = 2/3$, 30° wide barriers were very similar, while that with a 60° wide barrier was close to the transition seen in the unblocked annulus. *Figures 7.1* and *7.8* show a slight stabilizing effect on the waves compared with an unblocked annulus, as mentioned by *Leach (1975)*, though *Figure 7.12* does

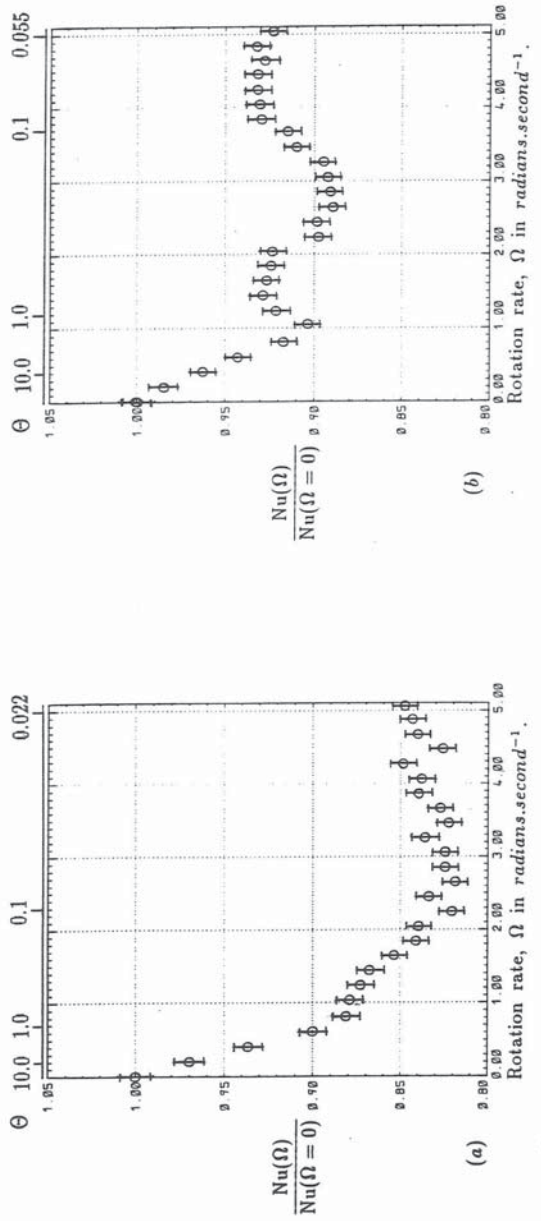

FIGURE 7.16: Measurements showing the dependence of Nusselt number, $Nu(\Omega)$, divided by $Nu(\Omega = 0)$, on Ω, for the system with a one-third partial barrier. (a) $\Delta T \approx 4\ K$, (b) $\Delta T \approx 10\ K$.

Run No	ΔT K	Ω $rad.sec^{-1}$	ΔT_{BAR} K	Prandtl No	Θ	Taylor No	Rayleigh No	Ekman No	$H_{conductive}$ $watts$	H_{total} $watts$	Nusselt No
228	4.00	0.000	0.12	13.95	∞	0	8.49×10^{6}	∞	1.53	16.32	10.70
229	4.01	0.000	0.13	13.95	∞	0	8.51×10^{6}	∞	1.53	16.35	10.70
230	4.02	0.203	0.14	13.95	1.29×10^{1}	1.90×10^{5}	8.54×10^{6}	1.46×10^{-3}	1.53	15.92	10.38
231	4.04	0.405	0.15	13.95	3.26	7.53×10^{5}	8.57×10^{6}	7.33×10^{-4}	1.54	15.43	10.02
232	4.00	0.606	0.16	13.95	1.44	1.69×10^{6}	8.49×10^{6}	4.89×10^{-4}	1.52	14.68	9.63
233	4.00	0.807	0.17	13.95	8.13×10^{-1}	2.99×10^{6}	8.49×10^{6}	3.68×10^{-4}	1.52	14.38	9.43
234	3.99	1.027	0.20	13.95	5.01×10^{-1}	4.85×10^{6}	8.48×10^{6}	2.89×10^{-4}	1.52	14.33	9.41
235	4.05	1.228	0.23	13.95	3.55×10^{-1}	6.93×10^{6}	8.59×10^{6}	2.41×10^{-4}	1.54	14.42	9.34
236	4.02	1.433	0.22	13.95	2.59×10^{-1}	9.44×10^{6}	8.53×10^{6}	2.07×10^{-4}	1.53	14.21	9.28
237	4.02	1.636	0.26	13.95	1.99×10^{-1}	1.23×10^{7}	8.54×10^{6}	1.81×10^{-4}	1.53	13.99	9.13
238	4.02	1.838	0.28	13.95	1.58×10^{-1}	1.55×10^{7}	8.53×10^{6}	1.61×10^{-4}	1.53	13.80	9.00
239	4.03	2.039	0.30	13.95	1.28×10^{-1}	1.91×10^{7}	8.56×10^{6}	1.45×10^{-4}	1.54	13.81	8.98
240	4.00	2.242	0.28	13.95	1.05×10^{-1}	2.31×10^{7}	8.49×10^{6}	1.32×10^{-4}	1.53	13.39	8.78
241	3.99	2.446	0.36	13.95	8.84×10^{-2}	2.75×10^{7}	8.48×10^{6}	1.21×10^{-4}	1.52	13.58	8.92
242	4.00	2.648	0.25	13.95	7.55×10^{-2}	3.22×10^{7}	8.49×10^{6}	1.12×10^{-4}	1.52	13.36	8.76
243	3.99	2.851	0.31	13.95	6.51×10^{-2}	3.73×10^{7}	8.48×10^{6}	1.04×10^{-4}	1.52	13.43	8.82
244	3.99	3.052	0.30	13.95	5.68×10^{-2}	4.28×10^{7}	8.48×10^{6}	9.72×10^{-5}	1.52	13.42	8.82
245	3.99	3.255	0.31	13.95	4.99×10^{-2}	4.87×10^{7}	8.48×10^{6}	9.11×10^{-5}	1.52	13.61	8.94
246	3.99	3.456	0.31	13.95	4.42×10^{-2}	5.49×10^{7}	8.47×10^{6}	8.58×10^{-5}	1.52	13.39	8.80
247	4.01	3.658	0.29	13.95	3.97×10^{-2}	6.15×10^{7}	8.52×10^{6}	8.11×10^{-5}	1.53	13.54	8.85
248	4.00	3.861	0.36	13.95	3.56×10^{-2}	6.85×10^{7}	8.50×10^{6}	7.68×10^{-5}	1.53	13.71	8.98
249	4.01	4.062	0.29	13.95	3.22×10^{-2}	7.58×10^{7}	8.51×10^{6}	7.30×10^{-5}	1.53	13.70	8.96
250	4.01	4.266	0.24	13.95	2.92×10^{-2}	8.36×10^{7}	8.52×10^{6}	6.95×10^{-5}	1.53	13.89	9.08
251	4.02	4.468	0.28	13.95	2.66×10^{-2}	9.17×10^{7}	8.53×10^{6}	6.64×10^{-5}	1.53	13.53	8.84
252	3.99	4.670	0.30	13.95	2.42×10^{-2}	1.00×10^{8}	8.48×10^{6}	6.35×10^{-5}	1.52	13.68	8.99
253	3.98	4.875	0.25	13.95	2.22×10^{-2}	1.09×10^{8}	8.46×10^{6}	6.09×10^{-5}	1.52	13.71	9.02
254	3.99	5.056	0.28	13.95	2.07×10^{-2}	1.17×10^{8}	8.48×10^{6}	5.87×10^{-5}	1.52	13.81	9.07

TABLE 7.5: Temperature and heat transport measurements with a one-third, 30° wide barrier.

Run No	ΔT K	Ω $rad.sec^{-1}$	ΔT_{BAR} K	Prandtl No	Θ	Taylor No	Rayleigh No	Ekman No	$H_{conductive}$ $watts$	H_{total} $watts$	Nusselt No
255	9.99	0.000	0.31	13.95	∞	0	2.12×10^{7}	∞	3.81	54.73	14.37
256	9.99	0.000	0.16	13.95	∞	0	2.12×10^{7}	∞	3.81	54.70	14.36
257	9.99	0.203	0.23	13.95	3.23×10^{1}	1.89×10^{5}	2.12×10^{7}	1.46×10^{-3}	3.81	53.92	14.15
258	10.01	0.405	0.26	13.95	8.08	7.54×10^{5}	2.13×10^{7}	7.32×10^{-4}	3.82	52.81	13.83
259	10.02	0.607	0.31	13.95	3.61	1.69×10^{6}	2.13×10^{7}	4.89×10^{-4}	3.82	51.74	13.54
260	10.05	0.808	0.27	13.95	2.04	3.00×10^{6}	2.13×10^{7}	3.67×10^{-4}	3.83	50.49	13.17
261	10.00	1.041	0.21	13.95	1.22	4.98×10^{6}	2.12×10^{7}	2.85×10^{-4}	3.81	49.48	12.98
262	9.98	1.238	0.30	13.95	8.62×10^{-1}	7.05×10^{6}	2.12×10^{7}	2.40×10^{-4}	3.81	50.36	13.23
263	9.98	1.442	0.38	13.95	6.36×10^{-1}	9.56×10^{6}	2.12×10^{7}	2.06×10^{-4}	3.80	50.77	13.34
264	9.97	1.642	0.41	13.95	4.90×10^{-1}	1.24×10^{7}	2.12×10^{7}	1.81×10^{-4}	3.80	50.64	13.31
265	9.97	1.844	0.49	13.95	3.89×10^{-1}	1.56×10^{7}	2.12×10^{7}	1.61×10^{-4}	3.80	50.48	13.27
266	9.98	2.032	0.59	13.95	3.20×10^{-1}	1.90×10^{7}	2.12×10^{7}	1.46×10^{-4}	3.81	50.46	13.26
267	10.05	2.235	0.46	13.95	2.67×10^{-1}	2.29×10^{7}	2.14×10^{7}	1.33×10^{-4}	3.83	49.44	12.90
268	10.05	2.438	0.47	13.95	2.24×10^{-1}	2.73×10^{7}	2.14×10^{7}	1.22×10^{-4}	3.83	49.51	12.91
269	10.06	2.641	0.47	13.95	1.91×10^{-1}	3.20×10^{7}	2.14×10^{7}	1.12×10^{-4}	3.84	49.05	12.73
270	10.03	2.847	0.43	13.95	1.64×10^{-1}	3.72×10^{7}	2.13×10^{7}	1.04×10^{-4}	3.83	48.98	12.80
271	10.03	3.047	0.48	13.95	1.43×10^{-1}	4.27×10^{7}	2.13×10^{7}	9.73×10^{-5}	3.82	49.01	12.82
272	9.97	3.251	0.44	13.95	1.25×10^{-1}	4.86×10^{7}	2.12×10^{7}	9.13×10^{-5}	3.80	48.88	12.86
273	9.96	3.455	0.62	13.95	1.11×10^{-1}	5.48×10^{7}	2.12×10^{7}	8.59×10^{-5}	3.80	49.63	13.07
274	9.96	3.658	0.55	13.95	9.86×10^{-2}	6.15×10^{7}	2.11×10^{7}	8.11×10^{-5}	3.80	49.91	13.14
275	10.04	3.832	0.50	13.95	8.99×10^{-2}	6.80×10^{7}	2.13×10^{7}	7.74×10^{-5}	3.80	50.72	13.35
276	9.99	4.035	0.50	13.95	8.07×10^{-2}	7.54×10^{7}	2.12×10^{7}	7.35×10^{-5}	3.78	50.60	13.37
277	9.99	4.229	0.48	13.95	7.35×10^{-2}	8.28×10^{7}	2.12×10^{7}	7.01×10^{-5}	3.78	50.62	13.38
278	9.99	4.445	0.53	13.95	6.65×10^{-2}	9.15×10^{7}	2.12×10^{7}	6.67×10^{-5}	3.78	50.63	13.38
279	10.00	4.640	0.58	13.95	6.15×10^{-2}	9.89×10^{7}	2.12×10^{7}	6.39×10^{-5}	3.81	50.80	13.32
280	10.00	4.828	0.52	13.95	5.64×10^{-2}	1.08×10^{8}	2.12×10^{7}	6.14×10^{-5}	3.79	50.71	13.39
281	10.02	5.032	0.54	13.95	5.24×10^{-2}	1.16×10^{8}	2.13×10^{7}	5.90×10^{-5}	3.82	50.67	13.26

TABLE 7.5 (continued).

not.

Velocity measurements with a $h/d = 2/3$, 30° barrier seem to suggest that the system splits into two regions. An upper region has strong prograde flow, with a topographically forced wave, while a lower region is fully blocked by the barrier. The amplitude of the topographically forced wave appears to increase with Ω, but above the barrier v appears to decrease with Ω.

With the $h/d = 2/3$ barrier the dependence of ΔT_B on Ω looked qualitatively similar to the behaviour observed with a full barrier. ΔT_B was somewhat larger, reaching a maximum value of about 40% of ΔT. There was also more structure in the dependence of ΔT_B on Ω.

The heat transport measured with the partial barriers was less than that seen with the fully blocked system, but more than the heat transport in unblocked systems. The $h/d = 2/3$ barrier system transported more heat than the $h/d = 1/3$ barrier system. Certain aspects of the heat transport with the $h/d = 1/3$ barrier system looked quite similar to the heat transport observed in the unblocked annulus; for example the dip in the heat transport observed as the transition for the onset of waves was being passed, and the rapid decline in heat transport with Ω at small Ω.

7.2 Discussion of results.

7.2.1 Simplified flow pattern.

The flow observed with the two-thirds partial barrier appears to consist of four main components: (1) a radial overturning in the region blocked by the barrier, (2) a horizontal circulation with vertical structure, also in the region blocked by the barrier, (3) time-dependent, aperiodic waves at higher Ω, and (4) a topographically forced wave above the top of the barrier. Thus the flow appears to be

very similar to that seen with a full barrier in the blocked lower region, with the addition of a topographically forced wave above the barrier. The two circulations seen in the lower region shall again be called the η and ζ-circulations. Apart from the waves these processes are represented in *Figure 7.17*.

All these processes cause radial motions in the fluid, and so might be expected to contribute to advective heat transport. *Figure 7.17* represents a useful simplification to the flows, in the same way as *Figure 3.12* did for the full barriers. However the use of this approach is limited to the two-thirds barrier, because that was the only case where ΔT_B was measured across the barrier.

7.2.2 Heat advection by the η-circulation.

The hypothesis is made that the barrier blocked flow in the lower region of the annulus can be considered in isolation from flow in the upper (unblocked) region. Thus the following analysis proceeds as if the lower region in the $h/d = 2/3$ barrier system were a fully blocked system, of constant depth $\frac{2}{3}d$. Since the barrier had an angular width of 30°, the angular half-width of the barrier, $\epsilon = \pi/12$ *rads*. In the same way as §3.2.3, it is possible to derive an expression for H_η,

$$H_\eta(\bar{r}, a = 0; t) \approx \frac{\bar{\rho}\bar{C}_p g\alpha\Delta T_B \Delta T d^2}{24\Omega} \cdot \frac{(\pi - \epsilon)}{\pi}, \qquad (7.1)$$

and where d is the height of the barrier. At small Ω the ζ-circulation was weakest, there were no waves, and the topographically forced wave was also weak. Since flow in the top region was virtually completely azimuthal (at small Ω) it could carry no heat radially (neglecting for the moment the possibility of heat transport through the Ekman layer that would be expected to form on the lid and base of the annulus and the top of the barrier), so once more it is to be expected that

$$H_{adv}(\bar{r}; \phi, z, t) \approx H_\eta(\bar{r}, a = 0; t).$$

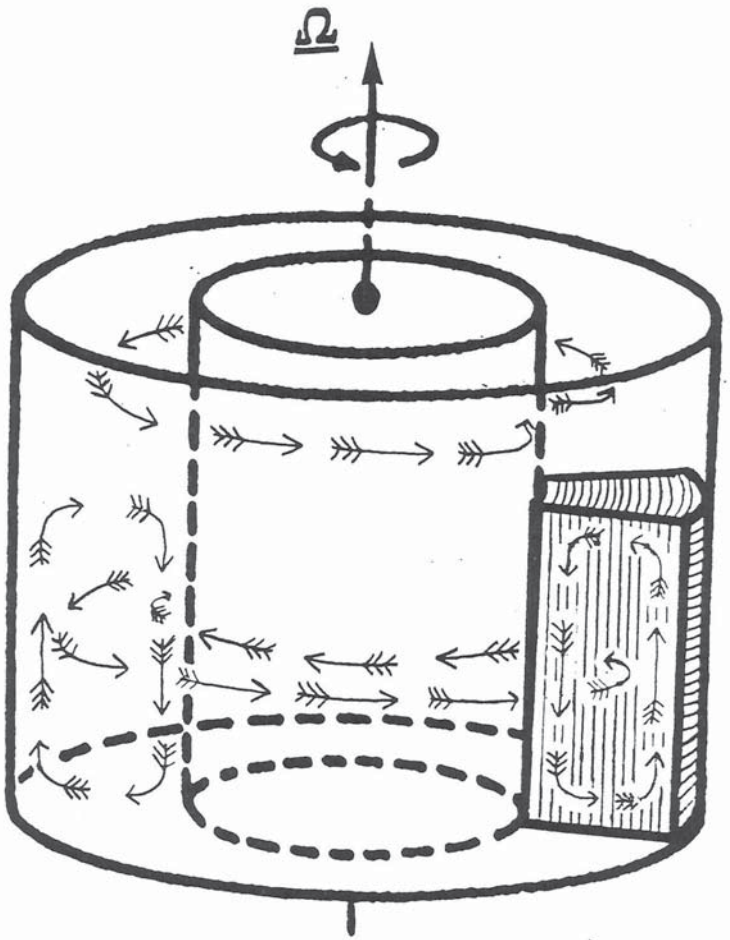

FIGURE 7.17: Diagram illustrating the simplified flow pattern representing fluid motion for the results described in section 7.1.1. The velocity measurements when there were no waves present are represented by the circulations shown by the arrows. The flow in the lower (blocked) part of the annulus is identical to that in the fully blocked system. In the upper region there is prograde flow with a topographically forced wave above the barrier.

So it is possible to re-define the quantity A_*, allowing for the thickness of the barrier, as

$$A_*^{-1} \equiv \frac{24\Omega H_{adv}(\bar{r}, a=0;t)}{\bar{\rho}\bar{C}_p g\alpha\Delta T_B \Delta T d^2} \cdot \frac{\pi}{(\pi-\epsilon)}. \tag{7.2}$$

Again it is expected that $A_* \sim 1$ at small Ω. *Figure 7.18* shows plots of A_*^{-1} against Ω, it can be seen that over a fair range of Ω $A_*^{-1} \approx 1.3$ which compares quite well with the value of 1.15 seen with the full insulating radial barrier. Comparison of *Figures 7.18* and *3.13* shows that they are both qualitatively rather similar, though with the partial barrier A_*^{-1} becomes significantly larger at high Ω than with the full barrier. Since $A_*^{-1} \approx H_{adv}/H_\eta$, then at 5.0 $rad.sec^{-1}$ with the full radial barrier, the total heat advection is about 2.2 times the heat advection by the η-circulation, while with the partial barrier, total heat advection at the same Ω is about 4 times that of the η-circulation. This increased advection is probably due to one or more of the following; (a) radial heat advection through the Ekman layers that form on the lid of the annulus and the top of the barrier, where v is very strong, (b) the fact that the time–dependent aperiodic waves might be able to transport heat over the entire depth of the system (rather than just the range of z blocked by the barrier), and (c) heat transport by the topographically forced wave.

The close agreement between *Figures 7.18* and *3.13* is sufficient to show that at low Ω heat advection in the partial barrier system is dominated by advection in the region blocked by the barrier, and the dynamics of that region are essentially very similar to the fully blocked system discussed in chapter 3. The results also support the idea that the flow in the blocked region can be considered in isolation from that in the upper unblocked region, at low Ω at least.

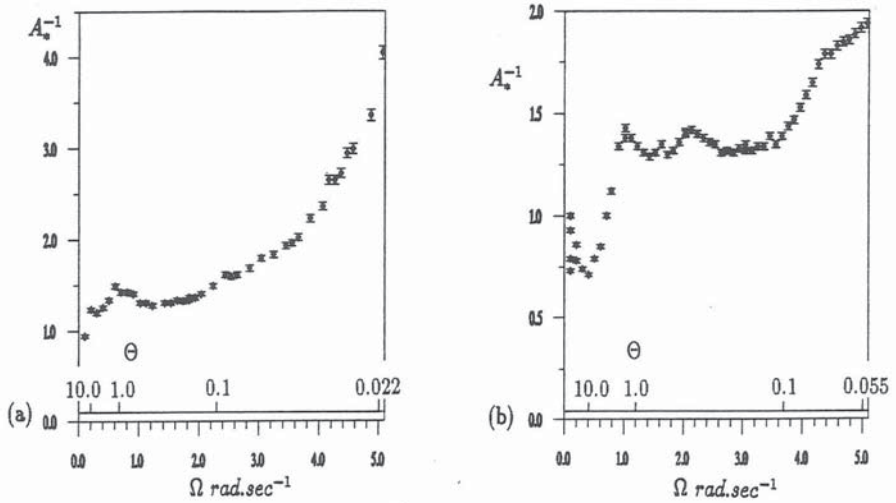

FIGURE 7.18: Plots of the dimensionless quantity A_*^{-1}, given in equation (7.2), for the measurements with a two-thirds 30° wide barrier. (a) $\Delta T \approx 4\ K$, (b) $\Delta T \approx 10\ K$. The results are quite similar to those with a full barrier, except that at high Ω, A_*^{-1} tends to be larger with the partial barrier.

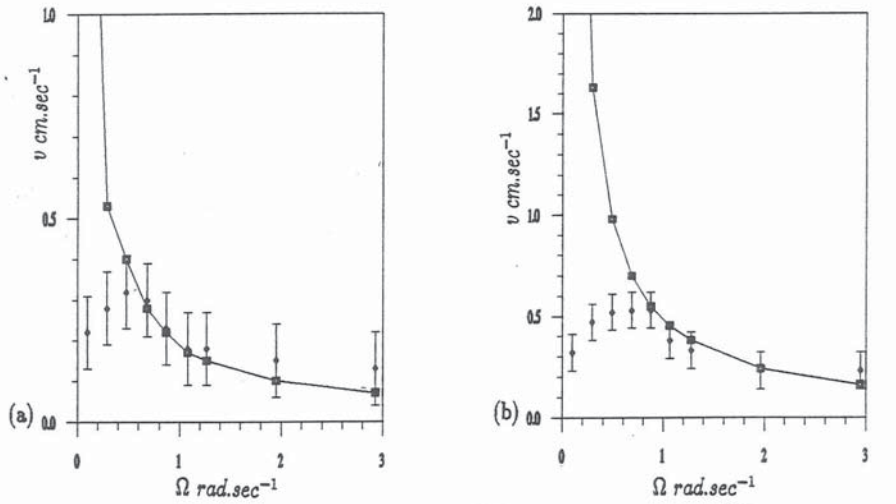

FIGURE 7.20: Plots of measurements of maximum v against Ω (points), and calculated v from equation (7.5) (squares joined by solid line), for the two-thirds partial barrier results. (a) $\Delta T \approx 4\ K$, (b) $\Delta T \approx 10\ K$. The line serves only as a guide for the eye.

7.2.3 Heat advection above the barrier.

The velocity results in the region blocked by the $h/d = 2/3$ partial barrier were very similar to those with the full barrier (chapter 3). Also the plots of A_*^{-1} were very similar in both cases (§7.2.2). These results suggest that the dynamics of the blocked region and the full barrier system were very similar. Thus it seems reasonable to estimate the heat advection by the blocked region of the $h/d = 2/3$ partial barrier system as two-thirds of the heat advection of the fully blocked system at the same values of Ω and ΔT. A similar approach could also be tried with the $h/d = 1/3$ partial barrier.

The heat advection of the blocked region was not calculated from the η and ζ-circulations because it was not clear what would be an appropriate value for ΔT_z, and also because the strength of the ζ-circulation was hard to estimate from the velocity measurements of v, due to the flow above the barrier. Estimating the ζ-circulation from the full barrier results would also be prone to error, because without understanding its mechanism, it would be unclear how a change of depth in the system might effect it.

If $H_{2/3}$ is the heat advection in the unblocked region above the $h/d = 2/3$, 30° wide barrier, and $H_{1/3}$ the similar quantity for the $h/d = 1/3$ barrier, then following the above,

$$H_{2/3} \approx (H_{adv})_p - \frac{2}{3}(H_{adv})_f, \quad \text{and} \quad H_{1/3} \approx (H_{adv})_p - \frac{1}{3}(H_{adv})_f,$$

where the subscripts 'p' and 'f' denote the appropriate partial barrier, and full barrier measurements respectively. Thus it is possible to define Nusselt numbers for the unblocked regions in the partial barrier systems as

$$\mathrm{Nu}_{2/3} \equiv \frac{H_{2/3} + \frac{1}{3}(H_{cond})_p}{\frac{1}{3}(H_{cond})_p}, \tag{7.3}$$

and

$$\mathrm{Nu}_{1/3} \equiv \frac{H_{1/3} + \frac{2}{3}(H_{cond})_p}{\frac{2}{3}(H_{cond})_p}, \tag{7.4}$$

where H_{cond} is the heat conduction through the system. The factors of $1/3$ and $2/3$ arise because only heat conduction through the unblocked part of the partial barrier system should be used. The estimate of the conductive heat transport is somewhat approximate, because the effect of the width of the barrier on H_{cond} has been ignored. Thus $\mathrm{Nu}_{1/3}$ and $\mathrm{Nu}_{2/3}$ provide an estimate of the Nusselt number for that part of the flow in the unblocked region above the partial barriers.

Figure 7.19 shows plots of $\mathrm{Nu}_{1/3}$ and $\mathrm{Nu}_{2/3}$ against Ω. Comparison can be made with *Figure 1.3*, which shows Nusselt numbers for flow in an unblocked annulus. It should be remembered that certain aspects of the two flows are fundamentally different, these are: the form of the waves (regular in the unblocked annulus at certain values of Ω, but time-dependent and aperiodic in the partial barrier measurements), and the appearance of a topographically forced wave in the partial barrier systems. Nonetheless the magnitudes of the Nusselt numbers in *Figures 7.19* and *1.3* are all fairly similar, and are consistent with the sorts of values seen in the previous experimental results. For the non-rotating annulus typical values for the heat transport were Nu$\approx$ 11 at $\Delta T \approx 4\ K$ and Nu$\approx$ 14 for $\Delta T \approx 10\ K$ (see *Tables 3.2* and *4.2*). Thus the technique used to estimate the heat transports in the unblocked regions above the partial barriers does appear to produceing Nusselt numbers of the appropriate size, leading to the conclusion that the method is perhaps not too inaccurate. The fact that (a) is quite similar to (c), and (b) to (d), despite the halving of the height of the barrier, also suggests that the method of calculation has a certain degree of consistency. These two considerations provide a certain degree of evidence that the method used to

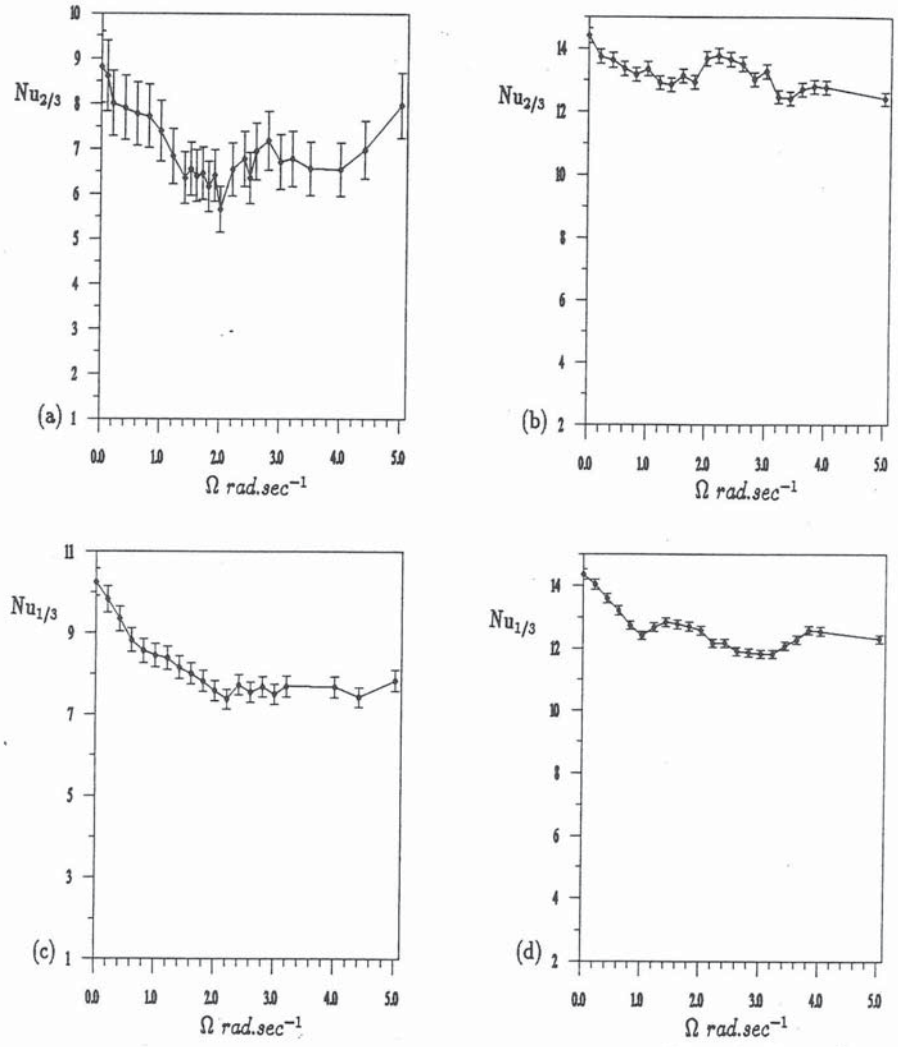

FIGURE 7.19: Plots of estimated Nusselt number for the unblocked regions of the partial barrier experiments. (a), (b) Two-thirds partial barrier results, $\mathrm{Nu}_{2/3}$ is given by equation (7.3). (c), (d) One-third partial barrier results, $\mathrm{Nu}_{1/3}$ is given by equation (7.4). (a), (c) $\Delta T \approx 4\ K$, (b), (d) $\Delta T \approx 10\ K$. The line serves only as a guide to the eye.

calculate *Figure 7.19* is probably fairly accurate.

Figure 7.19 (d) bears a strong qualitative resemblance to *Figure 1.3*, and in both cases Nu drops to about 80% of its non-rotating value when waves are present, despite the differences in the type of the waves. All the results also show a tendency for Nu to decrease sharply with Ω at small Ω, a result not seen with the full insulating barrier, but characteristic of measurements with an unblocked annulus system.

Figure 7.19 (a) shows signs of an upturn in the heat transport at high Ω. This is the only plot that shows such a marked difference from the heat transport results with an unblocked annulus. It is possible that this increase in heat advection is due to a topographically forced wave or some other effect associated with the partial barrier; if so, this is the only indication in the results of any significant heat transport by either a topographically forced wave or another process.

More detailed comparison could be made with heat transport measurements made using a system of the same depth as the unblocked regions of the partial barrier experiments, and with small topography of the same angular width as those barriers. It is not altogether clear what the height of that topography should be, for such a series of measurements, except that it should be high enough to stand well clear of the top of the lower Ekman layer, but small enough so that either a blocked region does not form, or if it does, it does not advect a significant amount of heat. *Davey (1978)* derives a quantity $\mu = \mathrm{Max}(\mathrm{Ro}, \mathrm{Ek}^{1/2})$, where Ro is the Rossby number (see equation (1.12)) and Ek is the Ekman number (equation (1.15)). $\mu = h_\mu/d$ where geostrophic flow can only pass over topography of height $\sim h_\mu$ in the direction of flow. Thus it seems reasonable to suppose that a barrier with h significantly greater than h_μ might cause the flow to split with z into a lower blocked region, and an upper region which would respond to the

topography as if it had a height of order h_μ. Taking the thickness of the Ekman layer as $\delta_{Ek} = (\nu/\Omega)^{1/2}$ (*Tritton (1988)*), then at $\Omega = 1\ rad.sec^{-1}$, h must be greater than about 1mm. Next, taking $v \sim 0.5\ cm.sec^{-1}$ at $\Omega = 1\ rad.sec^{-1}$ (from *Figure 7.20*), gives Ro$\sim$ 0.05, at a similar value of Ω, Ek$\sim 3 \times 10^{-4}$, so that $\mu \sim 0.05$, and $h_\mu \sim 0.7\ cm$. Thus for topography to stand clear of the Ekman layer and have no blocked region form, it should perhaps have a height of between about 1mm and 7mm.

However the results of *Figure 7.19* are sufficient to indicate that flow in the unblocked region above the barrier has more in common (with regard to its heat transport) with unblocked flows, than with fully blocked flows.

7.2.4 Fluid velocities above the barrier.

In the unblocked region of the $h/d = 2/3$, 30° wide barrier system, it is to be expected that the dependence of v on Ω and ΔT should be governed by the so-called 'Thermal Wind' equation (1.10), when radial geostrophic balance holds. Linearizing, and putting $\partial T/\partial r \approx \Delta T_r/(b-a)$, (1.10) can be written

$$v(z) \approx \frac{g\alpha}{2\Omega}.\frac{\Delta T_r}{(b-a)}(z - z_0),$$

where ΔT_r is the radial temperature difference across the interior of the fluid where radial geostrophic balance is assumed to hold, $\delta r \approx (b-a)$, and z_0 is the height in the annulus at which $v = 0$. Looking at *Figure 7.6* it is quite difficult to estimate a suitable value for z_0. Since radial geostrophic balance should hold at higher values of Ω, the level at which $v = 0$ in (c) is considered. Since the maximum values of v shall be used, and these occur towards the walls, the mean value of z_0 for the jets at each side was used. Hence $z_0 = 7.0\ cm$ was used, the mean of 9.7 cm and 4.3 cm, the approximate values seen beneath the

jets. The maximum values of v that were measured occurred at the top level where measurements were made, $z = 12.4\ cm$. The value of ΔT_r used was that suggested by *Hide (1967)* for axisymmetric flow in an unblocked annulus, being $\Delta T_r \approx \Delta T/3$. If this value proved to be appropriate that would provide another link between the flow in the unblocked region of the partial barrier experiments and flow in an unblocked annulus. Thus

$$v(z) \approx \frac{g\alpha\Delta T(12.4 - 7.0)}{6\Omega(b-a)}\ cm.sec^{-1}. \qquad (7.5)$$

Values of the maximum value of $v(z)$ are given in *Table 7.6* and plotted against the measurements of maximum v in *Figure 7.20.*

Agreement was only expected when radial geostrophic balance held to a good approximation, which according to the scaling argument of chapter 1 should be at $\Omega \gtrsim 1\ rad.sec^{-1}$. The figure indicates agreement between equation (7.5) and the measurements from about $0.7\ rad.sec^{-1}$ upwards. The excellent agreement suggests that the estimate of $\Delta T_r \approx \Delta T/3$ is quite accurate, and is consistent with the interpretation that the temperature field in the unblocked region of the $h/d = 2/3$ partial barrier system has a radial temperature gradient similar to that in an unblocked system.

It is not altogether clear how significant the apparent similarity of the radial temperature gradients in the two cases is in indicating that the flows were similar. However results by D.W.Johnson (private communication), which are shown in *Figure 1.4*, and results with the computer simulation of fully blocked flows *Figure 5.3* confirm similar measurements taken by *Bowden and Eden (1968)*, which indicate that fully blocked flows tend to have very small radial temperature gradients. This suggests that the unblocked region in the partial barrier system has a radial temperature gradient more typical of an unblocked system, than a fully

Run No	Ω $rad.sec^{-1}$	ΔT K	$v(z)$ from eqn.(7.5) $cm.sec^{-1}$	Maximum v $cm.sec^{-1}$
284	0.867	3.94	0.22	0.23
285	0.096	3.77	1.89	0.22
286	0.289	3.20	0.53	0.28
287	0.481	4.00	0.40	0.32
288	0.685	4.00	0.28	0.30
289	1.078	3.86	0.17	0.18
290	1.267	4.06	0.15	0.18
291	1.952	4.23	0.10	0.15
292	2.928	3.98	0.07	0.13
293	0.097	9.98	4.94	0.32
294	0.294	9.96	1.63	0.47
295	0.489	9.99	0.98	0.52
296	0.685	9.99	0.70	0.53
297	0.875	10.01	0.55	0.53
298	1.063	10.02	0.45	0.38
299	1.275	10.01	0.38	0.33
300	1.961	9.94	0.24	0.23
301	2.944	9.95	0.16	0.23

TABLE 7.6: **Measurements of maximum v for the two-thirds 30° wide partial barrier.**

blocked system.

7.3 Conclusions.

With the $h/d = 2/3$ barrier, the velocity measurements indicated that flow in the blocked region was very similar to the flow with a fully blocking barrier. In §7.2.2, the temperature and heat transport measurements were also shown to yield results very similar to those with a full radial barrier. Thus it seems

clear that the blocked flow in the $h/d = 2/3$ partial barrier system is essentially identical to the flow in the full barrier system.

Above the $h/d = 2/3$ partial barrier, in the unblocked region, estimates of the Nusselt number (§7.2.3) showed that the flow transported heat in a way which was quite similar to the unblocked annulus, once the differences in the flows had been taken into account. The fluid velocities in the unblocked region were shown to be consistent with those predicted by a radial geostrophic balance, with a radial temperature gradient similar to that given by *Hide (1967)* for axisymmetric flow in an unblocked annulus, but unlike that for a fully blocked flow. Thus the flow in the unblocked region of the two-thirds partial barrier system seems to hold much in common with flows in an unblocked annulus, once the topographically forced wave has been taken into account.

While only temperature data was available for the one-third partial barrier, Nusselt numbers calculated for the unblocked region above the barrier agreed quite closely with those calculated for the two-thirds barrier system. The results in *Figure 7.19 (d)* were qualitatively very similar to those with an unblocked annulus, *Figure 1.3*. This agreement suggests that flow in the unblocked region is rather like that in an unblocked annulus, once the differences in the wave types, and the topographically forced wave have been considered. Since the calculation of the Nusselt numbers for the unblocked region assumed that flow in the blocked region had the same heat transport properties as for the fully blocked systems, this also provides evidence that the flow in the blocked region of the one-third partial barrier system was like that of the fully blocked system.

The results from the two barriers seem to indicate that the transition between blocked and unblocked flows is essentially a continuous one, and can be estimated by considering the proportion of the system blocked by the barrier. In other words the heat advection through a partial barrier annulus, with a barrier of height h

can be estimated to a fair degree of accuracy as h/d times the heat advection through a fully blocked system of depth d plus $1 - h/d$ times the heat advection through an unblocked annulus of depth d, provided Ω and ΔT are the same in all cases.

The heat transport results with the $h/d = 1/3$, 30° wide partial barrier were very similar to those of *Leach (1975)* for his 'type C' topography (§2.1.1). However Leach attributed the increase in heat transport over the unobstructed case to the effect of the topographically forced wave. The results above seem to suggest that this is not the case, but that the increase arises because the range of z blocked by the barrier transports heat rather as if it were a fully blocked system, with the greater heat transport associated with such a system.

Kester (1966) had concluded that the transition was relatively abrupt, occuring at a barrier height of about $0.7d$. However, as mentioned in the introduction to this chapter, his heat transport and temperature measurements cannot be relied upon. His conclusion arose from the change he saw in the surface flow pattern when the barrier was $0.7d$ high. Since Kester saw regular waves, using barriers of negligible angular width, while only time-dependent aperiodic waves were seen in the experiments described in this chapter, it must be concluded that the form of the waves is more sensitive to the angular width of a partial barrier than to its height. Kester worked with a wide range of barrier heights, and saw only regular waves. The transition for the onset of waves for the 30° wide barriers used in this chapter seemed to be fairly independent of the barrier heights (compare *Figures 7.8* and *7.13*). However the transition with the 60° wide barrier occurred at a different location, see *Figure 7.12*. This tends to reinforce the conclusion that the waves are more sensitive to the angular width of a partial barrier, than its height. The transition for the onset of waves with the 1/3, $\Delta\phi = 30°$ barrier was very close to that observed by *Leach (1975)* for his similar 'type C' topography

(see §2.1.1).

Since the form of the waves (*i.e.* whether regular or not) in the unobstructed region of the partial barrier experiments might be expected to affect their heat transport properties, it is quite possible that the sharp change in the form of the regular waves that Kester saw might correspond to an abrupt change in the heat transport of the unblocked region. This might suggest that the nature of the transition from blocked to unblocked flows depends on the angular width of the barriers involved. However since the form of the waves might only be expected to have a significant effect in the unblocked region, the net effect this would have on the total heat advection of a partially blocked system could be quite small.

7.4 Further investigations.

Velocity measurements with the $h/d = 1/3$, 30° wide barrier could be analysed in the same way as §7.2.4 to estimate ΔT_r in the unblocked region for that system. Possibly measurements could also be made to see whether there was an η-circulation in the region blocked by the one-third barrier. Temperature and heat transport measurements, with a thermocouple on each side of the barrier would allow A_*^{-1} to be plotted, to see how similar its behaviour was to the full barrier experiments. It might also be possible to measure typical values of ΔT_z for the blocked region of the system. These measurements would (possibly) confirm the conclusions regarding the $h/d = 1/3$ barrier results.

Measurements of heat transport, using the same depth as the unblocked regions in the partial barrier experiments and small topography with the same angular widths, could be compared with *Figure 7.19*. This would allow the accuracy of the method employed to estimate the Nusselt numbers of the flow in the unblocked regions to be determined. The height of the small topography used should probably be that suggested in §7.2.3, i.e. between 1mm and 7mm.

It is interesting to see that the results of *Figures 7.2* to *7.4* are qualitatively very similar to those of *Davey (1978)*, even though the two–thirds partial barrier can hardly be regarded as small topography. The experiments correspond to his intermediate regime ($\mathrm{Ek}^{1/2} \sim \mathrm{Ro}$), which shows a region of possible flow reversal just downstream of the barrier, as in the experiments (see *Figure 1.5*). This similarity tends to support the idea that the flow with the two–thirds partial barrier splits into two regions; an upper region which sees small topography resting on a lower 'fully blocked' region. All this suggests that it might be worthwhile reconstructing and modifying Davey's model so that its results could be compared with experimental measurements taken using the small topography mentioned above. This would make it possible to see how well the model describes the topographically forced waves seen in the experiments.

Experimental measurements with small topography and sloping bases might indicate the amount of heat transported by the time-dependent aperiodic waves, if they could be supressed (see chapter 6).

Comparisons with Kester's work indicated that the form of the waves, and the location of the transition might be dependent on the width of the barriers. A series of measurements with barriers of the same height but differing angular widths would allow their effect to be determined.